Available online at www.sciencedirect.com

ScienceDirect

Underground Space 25 (2025) 54–73

www.keaipublishing.com/undsp

Research Paper

Tunneling beneath the pile-raft foundations of high-speed railways: Progressive arching deformation and pile settlement behavior

Botao Hu [a], Yao Shan [a,d,*], Yu Zhao [a,b], Binglong Wang [a], Shunhua Zhou [a], Giovanni S. Alberti [c], Wenjie Ma [d], Bettina Detmann [e], Laurent Briançon [f]

[a] *Shanghai Key Laboratory of Rail Infrastructure Durability and System Safety, Tongji University, Shanghai 201804, China*
[b] *National Key Laboratory of Green and Long-Life Road Engineering in Extreme Environment, Shenzhen University, Shenzhen 518060, China*
[c] *MaLGa Center, Department of Mathematics, University of Genoa, Genova 16146, Italy*
[d] *School of Civil Engineering, Lanzhou Jiaotong University, Lanzhou 730070, China*
[e] *Department of Civil Engineering, Faculty of Engineering, University of Duisburg-Essen, Essen 45141, Germany*
[f] *INSA Lyon, GEOMAS, UR7495, Villeurbanne 69621, France*

Received 31 January 2024; received in revised form 13 December 2024; accepted 24 December 2024
Available online 4 March 2025

Abstract

Due to the unclear mechanisms behind tunneling-induced deformation of pile-raft foundations, there are strict global restrictions on tunneling beneath embankments of high-speed railways. This study conducted a series of two-dimensional tunneling model tests to investigate the tunneling-induced deformation characteristics and mechanisms of pile-raft foundations. Soil displacement field and pile settlement were measured using particle image velocimetry and displacement transducers. The changes in soil displacement and the flexure of the pile-raft foundation in response to varying tunnel-pile distances, ground surface loads, and tunnel volume loss were analyzed. The results indicate that the tunneling-disturbed zone can be categorized into a loosened zone and an arch zone as identified by the propagation and separation of shear bands, with significant soil settlement occurring in the loosened zone. The maximum settlement of piles in a pile-raft foundation is greater than that in greenfield due to the larger loosened zone. However, the settlement width at the ground surface in pile-raft foundations is reduced due to the blocking effect of the piles. According to the relative position between the piles and the formed arch structure, three patterns of tunneling-ground-pile systems can be identified. As the tunnel-pile distance increases, the maximum settlement of the piles decreases. Increasing surface loads hardly affects the maximum settlement value of the pile, while the tunneling-induced arch zone expands significantly. This study provides a fundamental understanding of pile settlement behavior for tunneling beneath the pile-raft foundations of high-speed railways.

Keywords: Pile-raft foundation; Tunneling; Deformation behavior; Model test; Arching effect

1 Introduction

With the expansion of railway and metro networks, an increasing number of cases of tunneling beneath existing railway infrastructures have been reported worldwide, such as tunneling beneath the Shanghai-Nanjing High-speed Railway in Suzhou, China (Huo et al., 2011), and tunneling beneath the Beijing-Shanghai High-speed Railway in Jinan, China (Shan et al., 2021). Underpass tunneling can cause unforeseen subgrade settlement and track irregularities, which pose a direct threat to the operational safety of passing trains (Zhou et al., 2023; Shan et al., 2023; Wang et al., 2024). This is particularly urgent and prominent for high-speed railways (HSRs) because the maximum deformation criterion for an HSR track is only 2 mm (Shan et al., 2022) according to technical specifications in China (National

* Corresponding author at: Shanghai Key Laboratory of Rail Infrastructure Durability and System Safety, Tongji University, Shanghai 201804, China.
E-mail address: shanyao@tongji.edu.cn (Y. Shan).
Peer review under the responsibility of Tongji University

https://doi.org/10.1016/j.undsp.2024.12.004

Railway Administration of the People's Republic of China, 2017). To determine a reasonable distance for tunneling beneath HSRs, an understanding of the tunneling-induced deformation mechanisms and the characteristics of HSR subgrades is required.

Pile-raft foundations have been widely employed in HSRs to control post-construction subgrade settlement. The cushion layer between the piles and raft is used for convenience and low construction cost. This layer will separate the pile and raft, to regulate the distribution of subgrade load (Liu et al., 2022; Bhartiya et al., 2021). Tunneling beneath pile-raft foundations is inevitable in the practical projects, such as tunneling beneath the Shanghai-Nanjing Railway in Wuxi (Han, 2020). Tunneling-induced soil deformation is the key control factor to ensure the safety of the cross point. The schematic diagram of tunneling-induced soil settlement in pile-raft foundation is shown in Fig. 1. The tunneling-induced deformation characteristics depend on various design parameters, including tunnel-pile distance (Chiang & Lee, 2007; Ng et al., 2013), pile working load (Hong et al., 2015), structural stiffness of the foundation (Amorosi et al., 2014) and soil density (Cao et al., 2024). Giardina et al. (2015) demonstrated through model tests that the building response depends not only on the relative stiffness between the structure and the soil but also on the building's weight, which is often overlooked in current assessments. Additionally, the pile settlement behavior is affected by the connection types of pile-upper structure (Boonsiri & Takemura, 2015; Ng et al., 2014). In HSR pile-raft foundations, piles are unconnected to the raft; instead, a cushion layer between the piles and the raft helps alleviate the upper load from the subgrade. However, this layer and disconnection reduces the overall stability of the pile-raft foundation (Lu et al., 2020) and increases sensitivity to tunnel construction. While previous studies have mainly focused on the connected pile-upper structures, there is limited guidance available for risk assessments related to tunneling adjacent to the unconnected pile-upper structure.

The settlement of a pile foundation is significantly affected by the location of the piles within various areas of the tunneling-disturbed zone (Lim et al., 2023; Jongpradist et al., 2013). Research on the identification of the different risk level regions and scope of this disturbed zone is crucial for assessing the stability and serviceability of group piles adjacent to tunneling. Therefore, research on identifying and classifying the tunnel-disturbed zone has garnered widespread attention (Ong et al., 2007). Kaalberg et al. (2006) and Selemetas et al. (2005) proposed several relationships between soil displacement on the greenfield surface and the settlement of pile toes, depending on the position of the pile tip. Selemetas (2005) identified three zones in which the settlement of the pile toe may be greater than (zone A), equal to (zone B), or less than (zone C) the soil settlement on the greenfield surface. Research has shown that the extent of the tunneling-disturbed zone, which experiences significant settlement, is related to the tunnel burial depth and tunnel volume loss (Marshall et al., 2012; Hu et al., 2024). However, previous studies on the identification risk level region have mainly focused on natural foundations or soft clay, with limited research on tunneling-disturbed zones in pile-raft foundations.

Tunneling-disturbed zones exhibit different local deformation mechanisms within sandy soil, which are related to the development of arching effects (Franza et al., 2019; Zhao et al., 2021; Wu et al., 2022). Therefore, elucidating the evolution of such effects is crucial for ground and pile settlement assessment. According to the characteristics of soil deformation and stress transfer caused by tunneling, the tunneling-disturbed zone can be divided into three

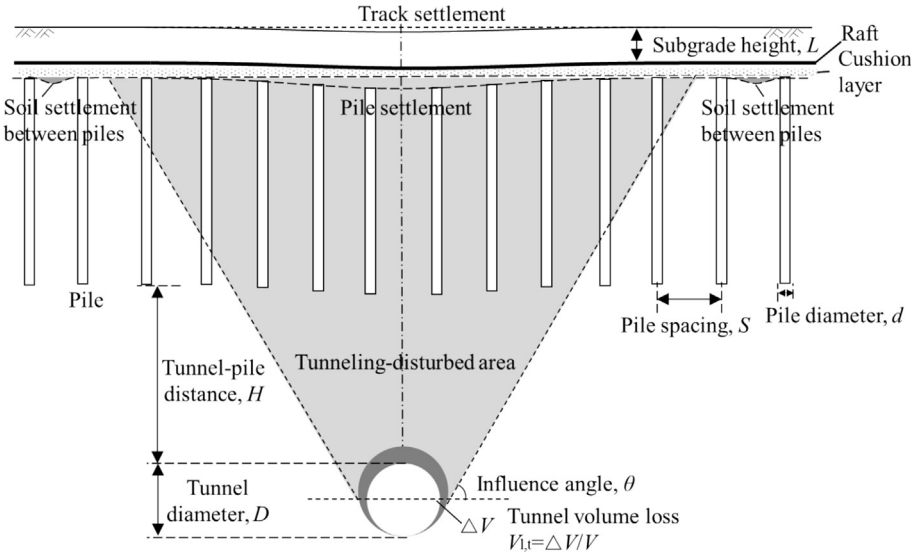

Fig. 1. Tunneling beneath a high-speed railway subgrade.

zones (Lin et al., 2019): the loosened zone, arch zone and undisturbed zone. Based on observed displacements, Lai et al. (2018) classified these deformed regions and explained that the interactions of rotational contact forces are the main reason for different soil arching structures and embankment deformations. The development of arching zone is affected by fill properties, filling height, and additional load on the surface (Rui et al., 2016; Khatami et al., 2019). However, previous research on arching effects has focused primarily on homogeneous strata or greenfield (da Silva Burke & Elshafie, 2021; Khatami et al., 2021, 2020), with limited studies on the progressive arching zone in pile-foundation systems and its impact on piled structures. Therefore, it is essential to study the tunneling-induced deformation characteristics of pile-raft foundations in conjunction with the arching effect for tunneling beneath pile foundations.

In this study, we investigated the tunneling-induced deformation characteristics of pile-raft foundations and examined the impact of progressive arching on pile settlement behavior, meanwhile, with emphasis on the effect of tunnel-pile distance and subgrade load on pile settlement and arching effect. To achieve these objectives, a model testing device for tunneling beneath pile-raft foundations was developed. The pile settlement, soil deformation and soil stress were measured in our tests. Benefiting from a comprehensive testing and analysis, this study elucidated the relationship between arching effects and pile settlement behavior. Further, different settlement patterns of tunneling-ground-pile systems can be identified, according to the relative position between the piles and the formed arch structure.

2 Model testing

2.1 Model testing apparatus

The device used in our tests consisted of a tunneling-ground-pile-raft model system and a data acquisition system, as shown in Fig. 2.

2.1.1 Tunneling-ground-pile-raft model system

The model system included a model box, a ground loss simulation system, and a pile-raft assembly. To balance operational space and the accuracy of soil displacement measurements, the experiment was scaled at 1:20. The model was designed based on pile-raft foundations of HSR with the following specifications: a subgrade height of 5 m, a pile diameter of 0.6 m for cement fly-ash gravel piles, a pile length of 6 m, and a pile spacing of 3 m. The shield tunnel had a diameter of 6 m. The scaling ratios for the main design parameters are listed in Table 1.

Cheng (2003) presented that the boundary of the tunneling-disturbed zone has an influence angle θ that is equal to $45° + \varphi/2$ (e.g., φ is the angle of internal friction

Table 1
Scale relationships in our model experiment.

Components	Physical quantity	Scaling ratio
Pile	Length, C_L	1:20
	Pile spacing, $C_s = C_L$	1:20
	Pile diameter, $C_d = C_L$	1:20
	Compressive rigidity, $C_{EA} = C_L^3$	$1{:}8 \times 10^3$
Tunnel	Tunnel diameter, $C_D = C_L$	1:20
Soil	Vertical earth pressure, $C_\sigma = C_L C_\gamma$	1:20

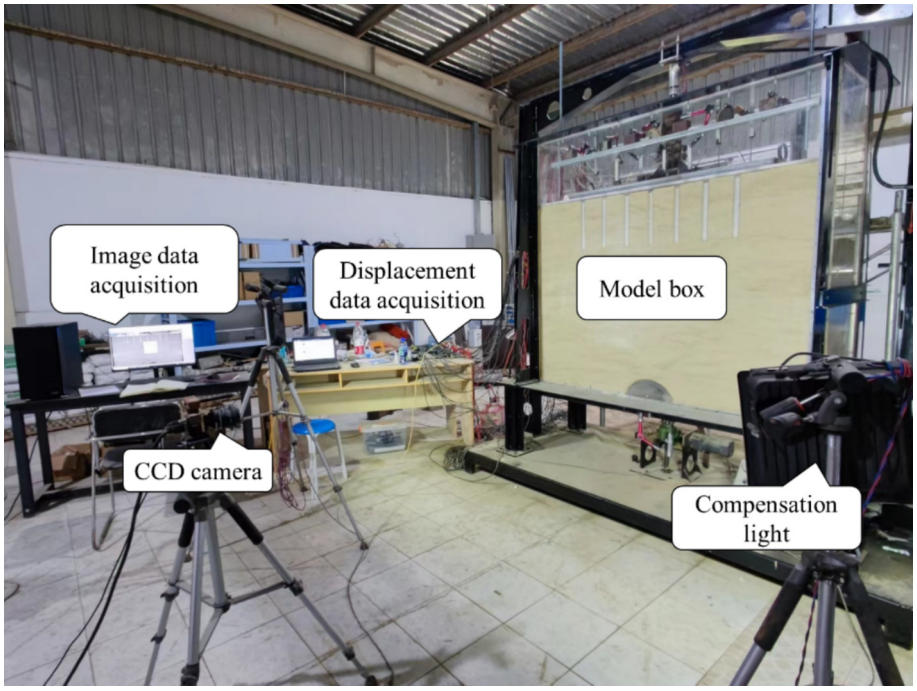

Fig. 2. Test equipment layout.

Fig. 3. Model apparatus. (a) Model box, and (b) model piles.

of the soil), which guided the design of the model box's height and length. As shown in Fig. 3(a), the model box dimensions were 1600 mm × 450 mm × 1600 mm.

For simulating ground loss, which is mainly distributed above the tunnel crown (Zhou, 2015), a tunnel-shaped trapdoor was employed. This trapdoor consisted of a flat acrylic plate and a semicircular acrylic plate, with a tunnel diameter of 300 mm and a length of 450 mm. The trapdoor was connected to a motor by a screw, allowing precise control via a digital display screen.

Considering the scaling ratio of the vertical compressive and bending stiffness values, aluminum pipe (elastic modulus, $E = 70$ GPa) is often utilized to simulate vertical loading piles (Franza & Marshall, 2018). In our study, the length of the aluminum pipe was 300 mm, the diameter was 30 mm, and the wall thickness was 3 mm. Because the surface of the aluminum pipe is smooth while that of an engineering pile is rough, granular sand was attached to the pipe surface in our tests to increase pile side friction (Franza & Marshall, 2019; Boonsiri & Takemura, 2015), as shown in Fig. 3(b).

Because piles are not connected in the rafts of pile-raft foundations, a pile group and loading plate were used to simulate the pile-raft structure in our tests. The subgrade load was applied to the pile-raft foundation through a jack. Holes were drilled in the loading plate to facilitate the installation of displacement transducers.

Half-sections of piles are often used to investigate pile-soil interactions (Yuan et al., 2017, 2013). To observe the tunneling-induced soil displacement field of the pile-raft foundation in our tests, the model piles were machined into half-sections along their vertical axes. The machined faces of the piles were placed against the acrylic front panel. The pile spacing was 150 mm, and four rows of piles were arranged along the width of the model box. Seven piles were placed along the length of each row. Therefore, a total of 28 piles were buried. Piles 1–4 were distributed from the tunnel center to the outside of the tunnel. The distance between the side piles and the model box was 335 mm, which was more than 10 times the pile diameter. As a result, the influence of the model box on the pile foundation was negligible (Bolton et al., 1999).

2.1.2 Data acquisition system

Pile settlement was measured by linear variable differential transformer (LVDT). The maximum measurement value of the LVDT was 100 mm and the accuracy was 0.01 mm. To measure the variation in the vertical stress distribution, 10 pressure sensors (with a diameter of 16 mm) were placed on the soil body, as shown in Fig. 4. The capacity and sensitivity coefficient of the stress sensors were 50 kPa and 2.1, respectively.

Soil displacement was measured using particle image velocimetry (PIV) technology, which is based on image recognition technology and can accurately measure the position of a target point in an image. In our experiments, the PIV system consisted of a high-speed charge-coupled device camera (CCD camera), two compensation lights, and image data analysis software. The resolution of the CCD camera was 2456 × 2056 pixels, and the sampling frequency of image acquisition was 4 Hz. Through the image analysis process, the displacement field was obtained based on image correlation matching, and the actual particle displacement was determined by converting pixel coordinates into physical coordinates. Agreement between pile displacement data obtained from the PIV and the LVDT systems on the pile caps confirmed the accuracy of the PIV system, as shown in Fig. 5.

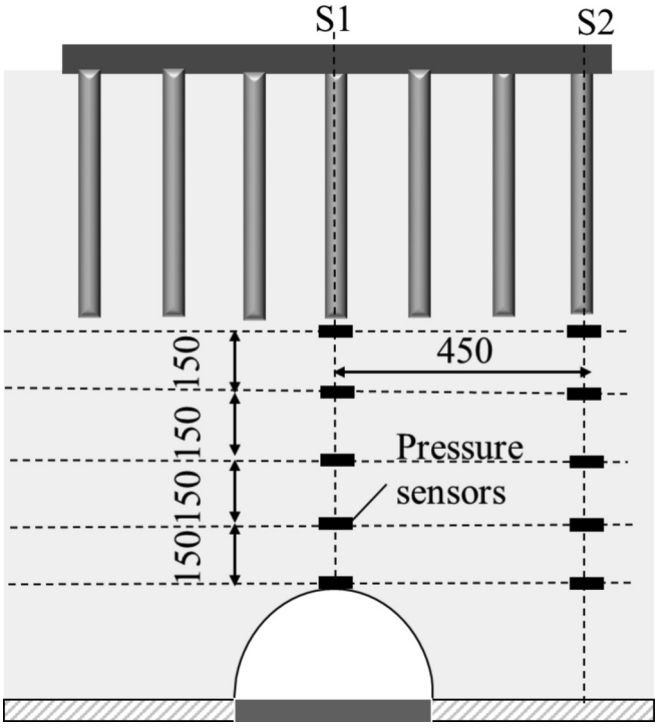

Fig. 4. Layout of the pressure sensors. (Unit: mm)

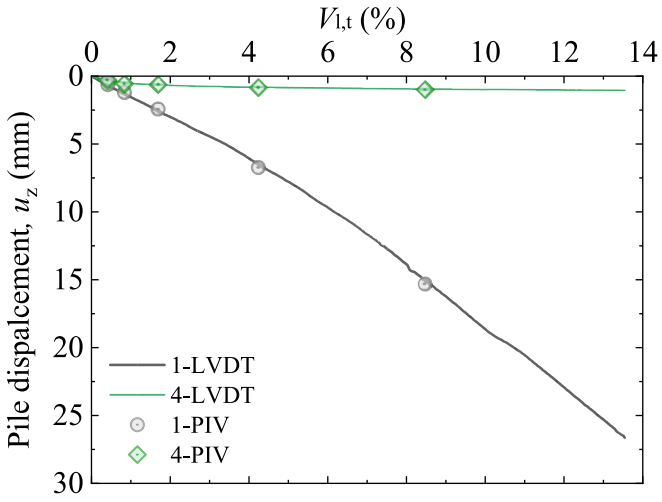

Fig. 5. Comparison of measurement data from PIV and LVDTs.

2.2 Material properties

Fujian Pingtan sand, a standard sand in China, was used in the tests. The basic physical and mechanical properties of this sand are listed in Table 2. The particle size of the sand ranges from 0.05 to 1.00 mm, and the size distribution of sand is presented in Fig. 6. The soil in the model box was filled in layers with a thickness of 15 cm. The soil relative density was 70%, and the angle of internal friction of the soil (φ) was 31.55°, as measured through triaxial tests.

Table 2
Physical and mechanical properties of the sand sample.

Properties	Value
Maximum dry density ρ_{dmin} (g/cm^3)	1.768
Minimum dry density ρ_{dmin} (g/cm^3)	1.466
Specific gravity G_s	2.655
Relative density D_r (%)	0.7
Angle of shear resistance of the sand (°)	31.55
Moisture content ω (%)	0

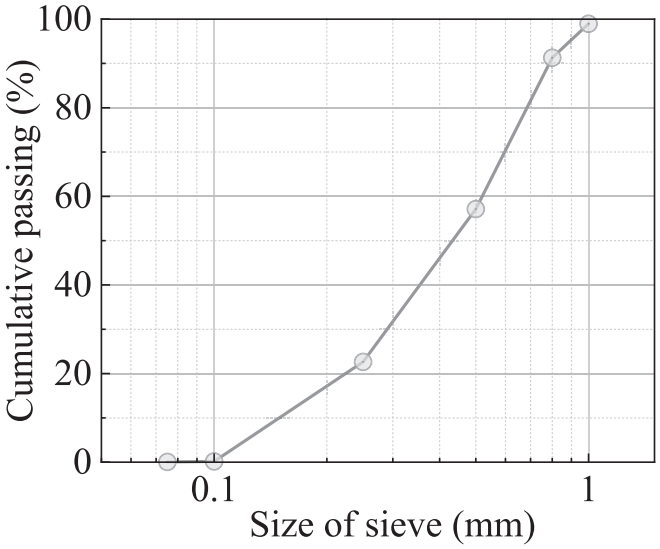

Fig. 6. Particle size distribution of Fujian Pingtan sand.

2.3 Testing plan and procedure

To investigate the effects of the distance between the tunnel and pile tip (H) and ground surface load (P) on the displacement of the pile and soil, six groups of tests were designed in addition to a greenfield test for comparative testing, as shown in Table 3. H/D is the normalized tunnel-pile distance through the tunnel diameter (D). The tunnel volume loss ($V_{l,t}$) is the ratio of the difference between the excavated volume and completed volume of the tunnel (ΔV) over the tunnel volume (V) (i.e., $V_{l,t} = \Delta V/V$, see Fig. 1). According to a previous study (Wei, 2010), most tunnel volume loss ($V_{l,t}$) values range from 0.13% to 4.30% depending on the tunnel construction method, soil properties, and tunnel bur-

Table 3
Model testing matrix.

Test No.	Foundation type	H/D	P (kPa)
1	Pile-raft	0.5	5
2		1.0	5
3		2.0	5
4		2.5	5
5		1.0	0
6		1.0	10
7	Greenfield	1.0	0

ial depth. In our tests, $V_{l,t} = 0.84\%$ was selected for low tunnel volume loss, and $V_{l,t} = 8.48\%$ was selected for extremely high tunnel volume loss, which corresponded to trapdoor displacements (δ) of 2 and 20 mm, respectively. High tunnel volume loss was included for cases in which tunnel boring machines do not achieve the target tunnel volume loss.

The detailed steps of testing were as follows:

(i) The model test material preparation included sand drying and applying lubricant to the sidewalls of the model box.
(ii) The sand was filled into the model box in layers with a thickness of 15 cm and pressure sensors were placed on the soil surface. When the soil layer reached the elevation of the pile tip, the model piles were buried (Fig. 7(a)) and the soil continued to be filled using the air pluviation method to the designed elevation (Fig. 7(b)).
(iii) The loading plate was placed and the LVDTs were installed above the piles (Fig. 7(c)). A jack was used to load the soil surface (Fig. 7(d)).
(iv) A monitoring system was installed and a high-speed CCD camera was set up in front of the model box and connected to a computer. After the trapdoor was moved downward, the soil displacement and pile settlement were recorded.

3 Experimental results and analysis

3.1 Settlement characteristics of the pile-raft foundation induced by tunneling

Figures 8 and 9 present the tunneling-induced contour of soil displacement and shear strain in the greenfield and pile-raft foundation. The vertical axis represents the distance between the soil and the bottom of the model box, while the horizontal axis represents the distance between the soil and the model box. As shown in Figs. 8(a) and 9(a), the tunneling-disturbed zones in the greenfield and pile-raft foundation are similar when $V_{l,t} = 0.84\%$, with soil settlement concentrated in the area above the tunnel. The tunneling-induced shear bands in the pile-raft foundation

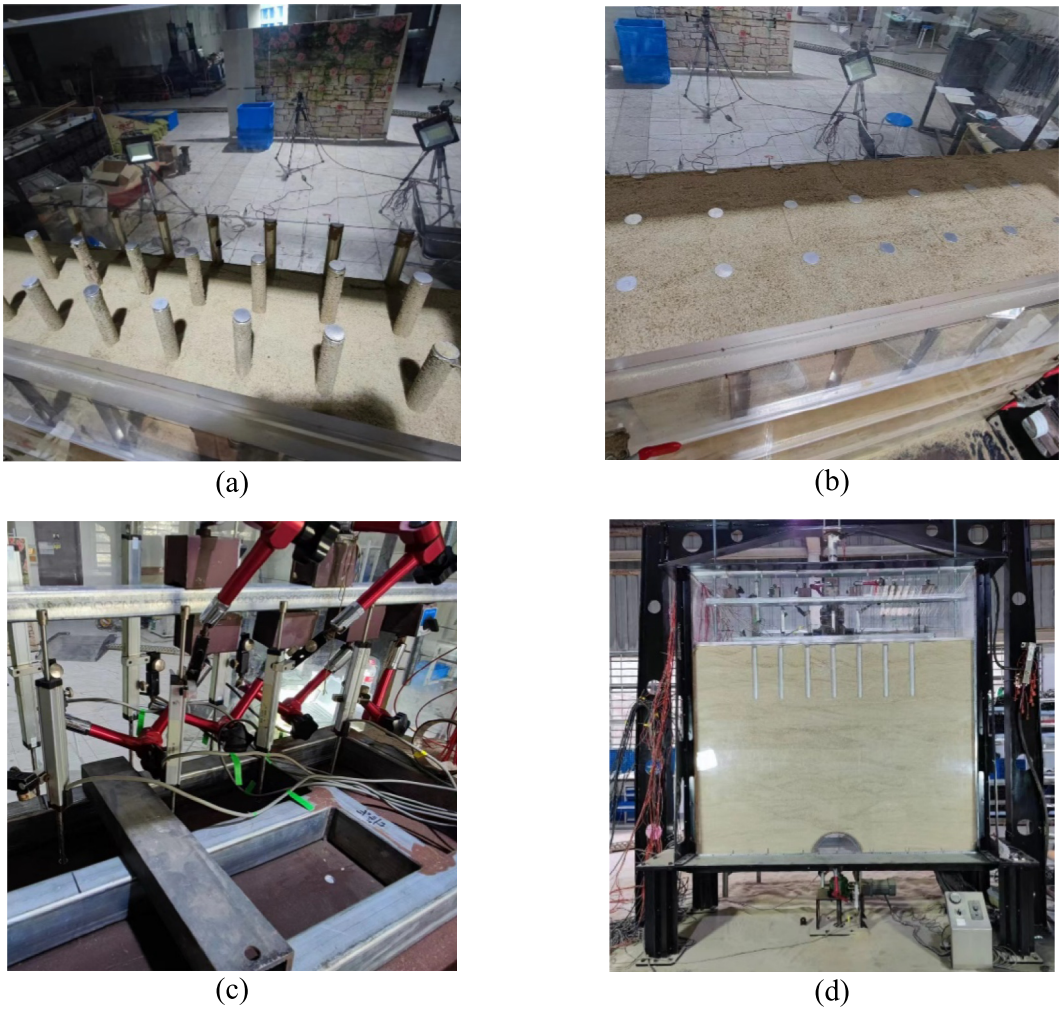

Fig. 7. Testing process. (a) Pile embedment, (b) soil filling completed, (c) LVDT layout, and (d) layout completed.

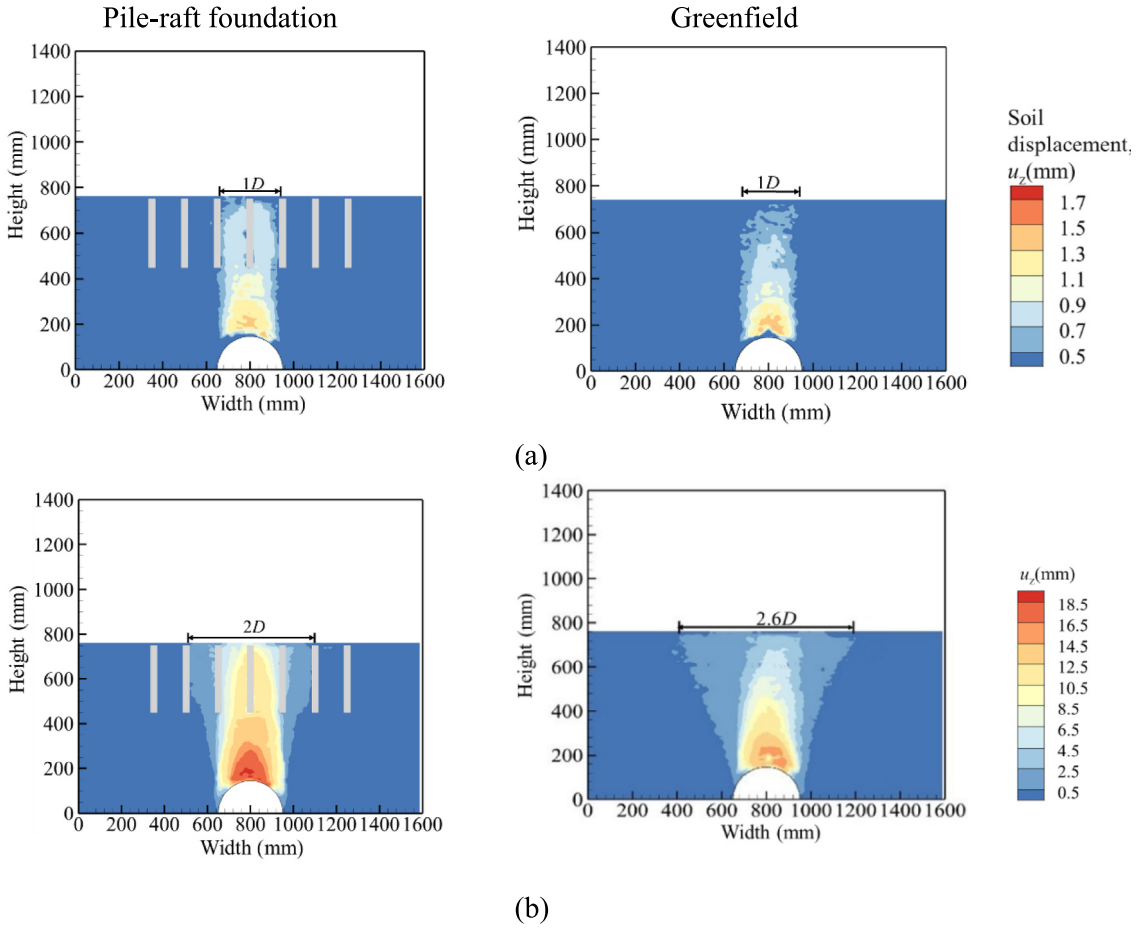

Fig. 8. Displacement fields for two types of foundation. (a) $V_{l,t} = 0.84\%$, and (b) $V_{l,t} = 8.48\%$.

extend vertically from the tunnel crown to the ground surface and the settlement width of the ground surface is $1D$.

The tunneling-disturbed zone expands with increasing $V_{l,t}$. Due to the blocking effect of the pile group, the tunneling-disturbed zone in the pile-raft foundation is less than that in the greenfield when $V_{l,t} = 8.48\%$. As shown in Fig. 9(b), the tunneling-induced shear bands near the surface curve to the outside of the tunnel extend from the tunnel crown to the ground surface, and the settlement width of the ground surface in the pile-raft foundation is $2D$.

According to the characteristics of soil deformation and stress transfer caused by tunneling, the tunneling-disturbed zone has been divided into three zones by Lin et al. (2019): loosened zone, arch zone, and undisturbed zone. The deformation of soil in the loosened zone was significantly affected by tunneling, which results in the loosened soil. Tunneling has a limited effect on soil displacement within the undisturbed zone. The soil settlement in the arch zone is significantly less than that in the loosened zone.

Figure 9(b) shows two clear shear bands extending from the tunnel to the ground surface, marked with a red dotted line. According to the soil deformation field shown in Fig. 8(b), large settlement occurs in the area below the red dotted line, indicating that this area is the loosened zone. The arch zone is the area inside the tunnel-disturbed zone but outside the loosened zone. As shown in Fig. 9(b), the arch zone in the pile-raft foundation is smaller than that in the greenfield when $V_{l,t} = 8.48\%$, while the loosened zone is larger than that in the greenfield.

The magnitude of ground loss is commonly expressed by two parameters: tunnel volume loss ($V_{l,t}$) and soil volume loss ($V_{l,s}$) (Franza et al., 2019). The concept of ground volume loss is illustrated in Fig. 10. Soil volume loss is defined as $V_{l,s} = V_S/V_0 \times 100$, where V_S is the volume of the settlement trough per unit length of the tunnel and V_0 is the notional final area of the tunnel cross-section. In Fig. 10, $u_{z,max}$ is the maximum soil displacement at the elevation of h.

Figure 11 presents the settlement troughs at different elevations (h) in two types of foundations. The maximum settlement values of the settlement trough gradually decrease with increasing h. When $V_{l,t} = 0.84\%$, the settlement trough in different h were similar under different foundation types. The maximum settlement and the settlement width increase with the increasing $V_{l,t}$. The settlement width in the greenfield is similar to that in the pile-raft foundation when $V_{l,t} = 8.48\%$, while the maximum soil settlement in pile-raft foundation is larger than that in the greenfield due to the larger loosened zone, as shown in Fig. 9(b).

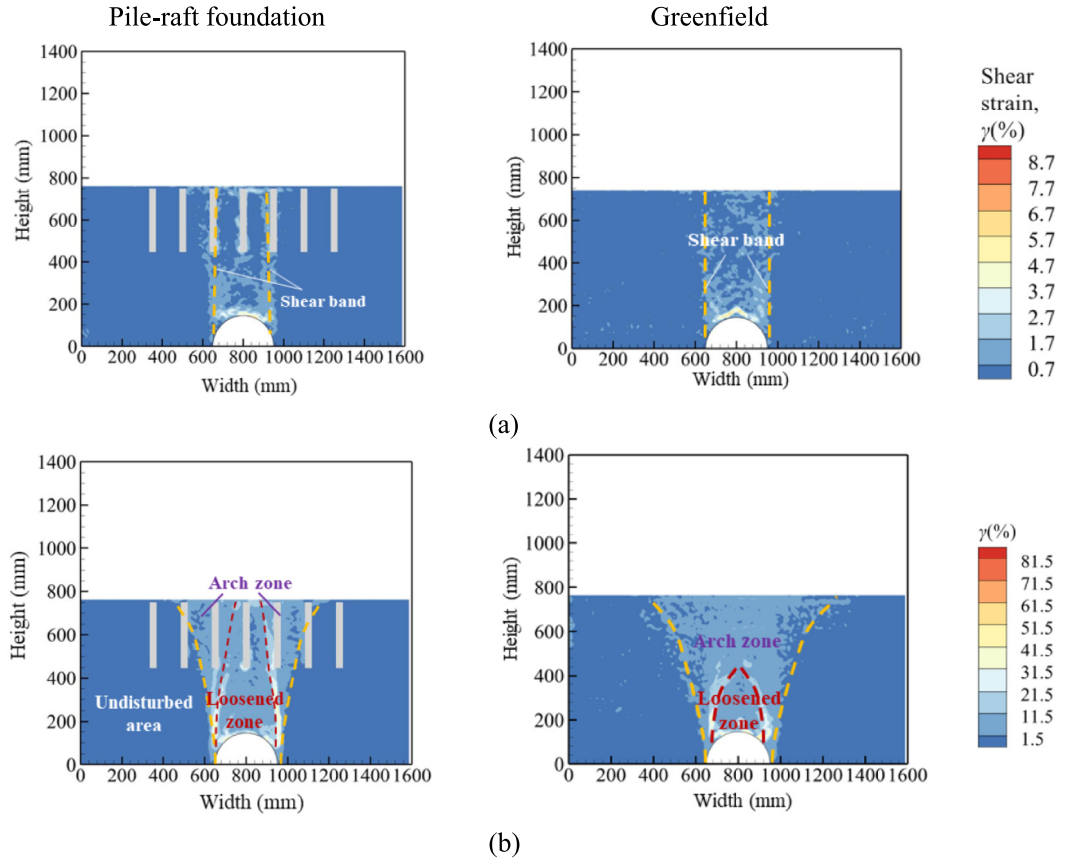

Fig. 9. Shear strains for two types of foundation. (a) $V_{l,t} = 0.84\%$, and (b) $V_{l,t} = 8.48\%$.

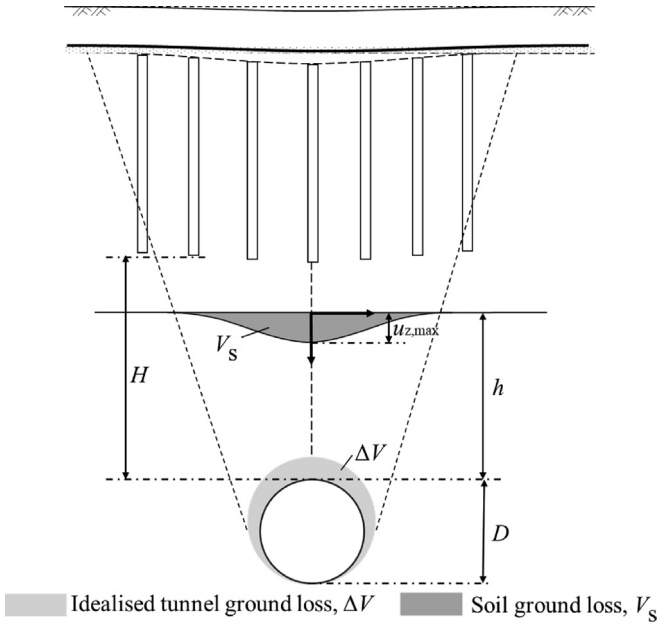

Fig. 10. Illustration of soil and tunnel volume loss.

Figure 12(a) presents the vertical settlement along the elevation of the tunnel centerline. The soil settlement gradually decreases with the increasing h. When $V_{l,t} = 0.84\%$, the tunneling-induced vertical settlement in the pile-raft foundation is similar to that in the greenfield, which was consistent with the results shown in Fig. 11(a). However, when $V_{l,t} = 8.48\%$, the vertical settlement in the greenfield is significantly smaller than that in the pile-raft foundation. This indicates that the greenfield enhances the arching effect to a certain extent and is more effective in preventing soil settlement in high tunnel volume loss. The soil volume loss gradually decreases with increasing h (as shown in Fig. 12(b)), which is related to the dilatancy characteristics of the soil (Franza et al., 2019).

3.2 Effects of tunnel-pile distance

Figure 13(a) presents the tunneling-induced soil displacement fields at different H/D in $V_{l,t} = 0.84\%$. For $H/D \leq 1.0$, the soil deformation pattern extends vertically from the tunnel crown to the surface, and the settlement width of the ground surface is $1D$. For $H/D \geq 2.0$, the pile foundation is outside the tunneling-disturbed zone and the shape of the tunneling-disturbed zone resembles a tower, indicating the formation of an arch.

With the increasing H/D, the soil deformation pattern gradually changes from a trumpet to a funnel and the settlement width is similar to the range of pile-raft structure, as shown in Fig. 13(b).

Figure 14(a) presents the tunneling-induced shear strain filed at different tunnel-pile distances when $V_{l,t} = 0.84\%$.

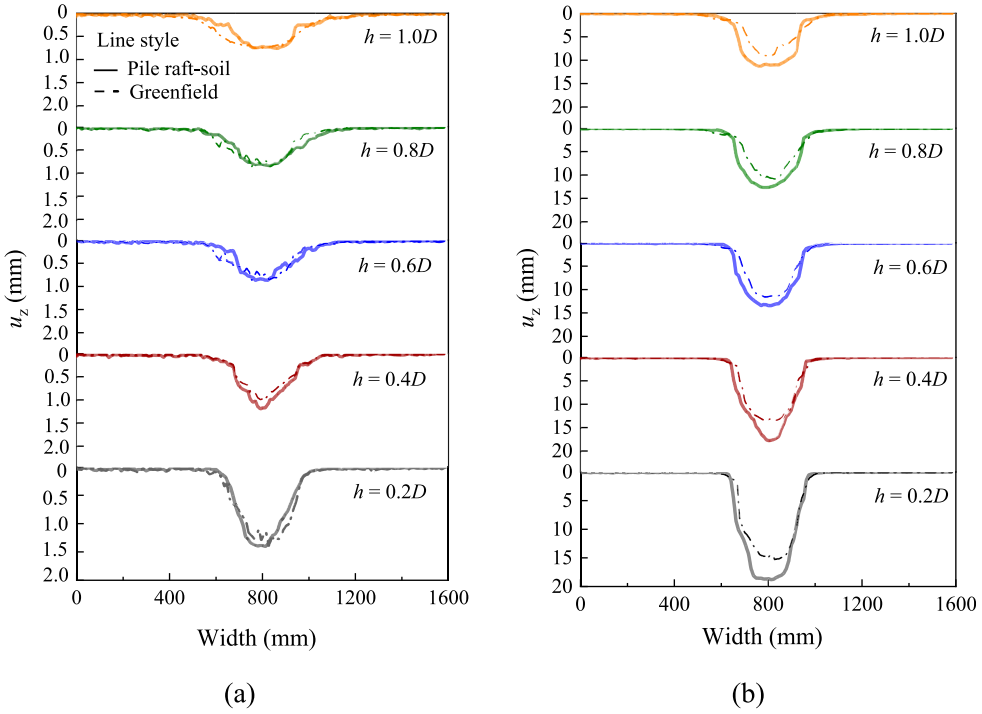

Fig. 11. Settlement trough at different h. (a) $V_{l,t} = 0.84\%$, and (b) $V_{l,t} = 8.48\%$.

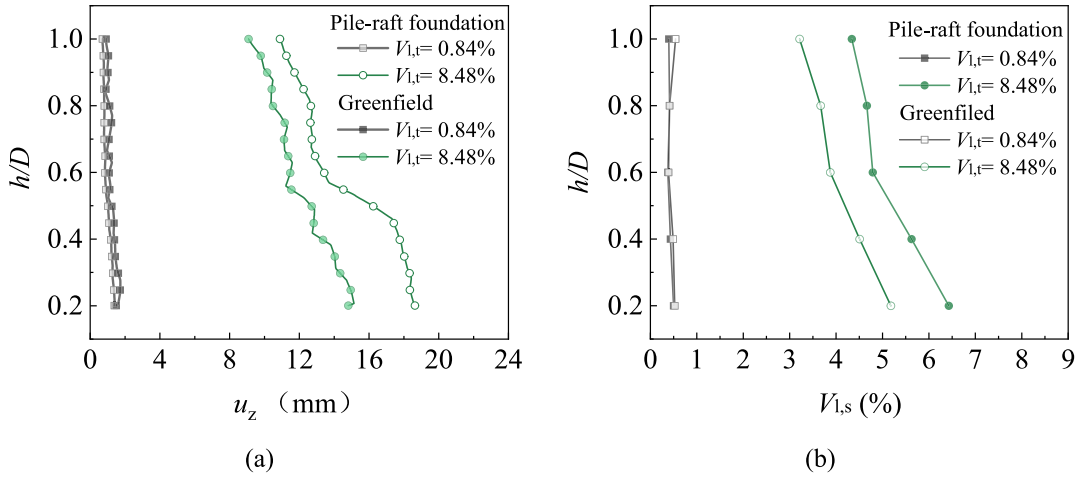

Fig. 12. Comparison of the vertical displacement of soil under different foundation types. (a) Vertical settlement with the elevation of the tunnel centerline, and (b) variation of $V_{l,s}$ with elevation.

Shear bands appear above the tunnel and develop vertically upwards when $H/D \leq 1.0$. The shear band curves tend to the inside of the tunnel with the increasing H/D. As shown in Fig. 14(b), the arch zone expands with the increasing H/D. When $H/D \leq 1.0$, the range of the loosened zone extends to the ground surface. With the increasing H/D, the height of the loosened zone decreases due to the increasing confining stress (da Silva Burke & Elshafie, 2021). When $H/D \geq 2.0$, two clear shear bands form an arch structure above the tunnel, and the piles are in the arch zone. The height of the loosened zone is roughly $1D$ when $H/D = 2.0$, which remains essentially unchanged with a further increase in H/D.

Figure 15 presents the settlement troughs at the pile tip elevation at different H/D. As H/D increases, the soil settlement at the pile tip elevation decreases rapidly, and the width of the settlement trough increases.

Figure 16 presents the evolution of pile settlement with $V_{l,t}$ at different H/D. Pile 1 is at the tunnel centerline, and pile spacing is $0.5D$. It can be observed that within the $1.0D$ range of the tunnel centerline (Piles 1 and 2), the pile settlement decreases rapidly with the increasing H/D, while outside the $1.0D$ range (Piles 3 and 4), the pile foundation settlement increases with the increasing H/D. Therefore, Piles 1 and 2 are called the inner-side piles, and Piles 3 and 4 are called the outer-side piles.

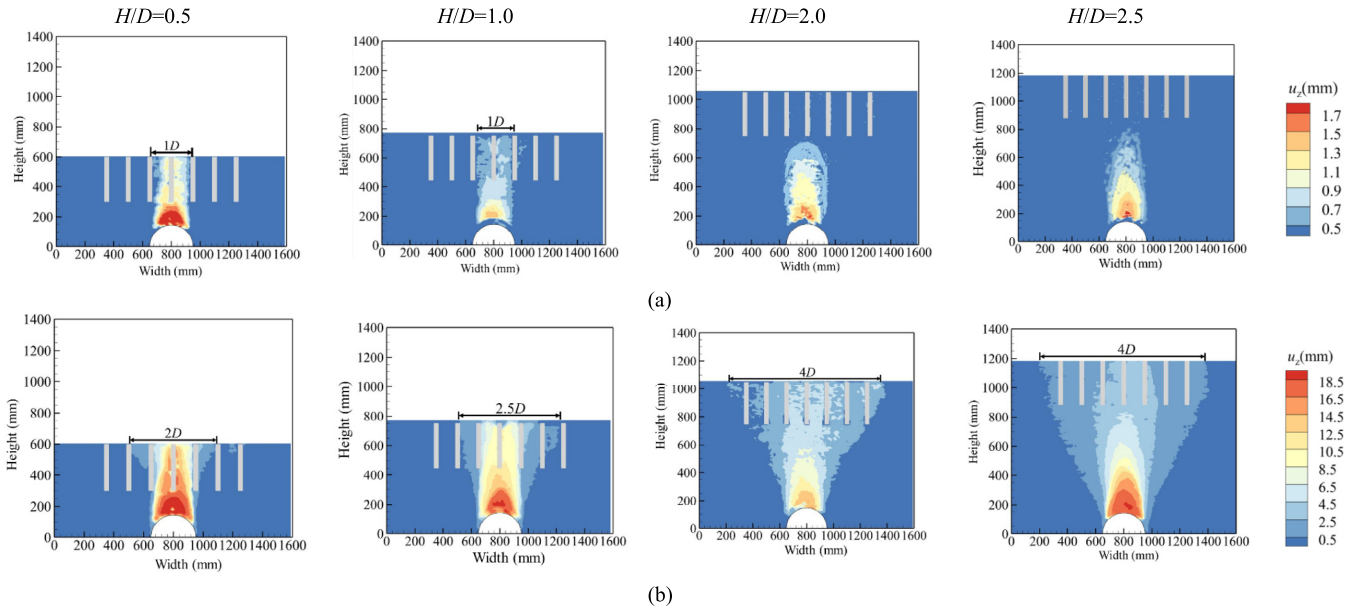

Fig. 13. Displacement fields at different H/D values. (a) $V_{l,t} = 0.84\%$, and (b) $V_{l,t} = 8.48\%$.

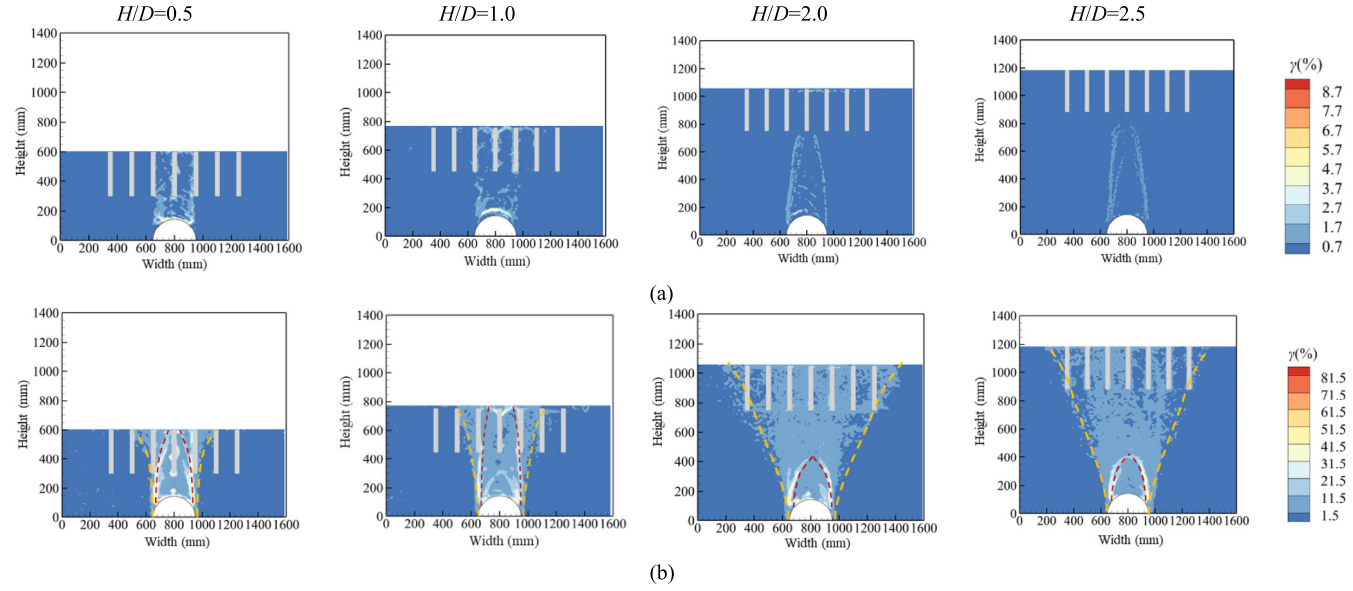

Fig. 14. Shear strain field at different H/D values. (a) $V_{l,t} = 0.84\%$, and (b) $V_{l,t} = 8.48\%$.

Figure 17(a) presents the evolution of inner-side pile settlement with $V_{l,t}$ for different H/D. Comparing the settlement rate of pile foundations and tunnel-shaped trapdoor through a 1:1 line, the settlement of piles can be divided into two stages. In the initial stage, the pile settlement rate was much lower than the trapdoor displacement rate. Zhao et al. (2021) suggested that this period is the initial and maximum arching stages. In the second stage, the loosened zone develops upwards with the increasing $V_{l,t}$, causing greater deformation of the soil around the pile, which leads to an increase in the settlement rate of the pile foundation. When the range of the loosened zone expands to the pile tip, the pile settlement curve reaches the 1:1 line. As seen in Fig. 17(a), the Pile 1 settlement curve does not reach the 1:1 line during the trapdoor displacement when $H/D \geq 2.0$, which indicates that piles are always in the arch zone. For outer-side piles, the settlement behavior with $V_{l,t}$ is presented in Fig. 17(b). The pile settlement rate was lower than the trapdoor displacement rate, and a small reduction in the pile settlement rate with $V_{l,t}$ can be shown. This reduction was attributed to the slippage between pile and soil, and additional shearing strains at the soil-pile interface. The outer-side pile settlement increases with the increasing H/D due to the larger tunneling-disturbed zone.

Figure 16 reveals that the settlement of each pile was different within the same test. Therefore, uneven settlement inevitably occurs in the pile-raft foundation. To evaluate the uneven settlement of piles, we propose a simple and

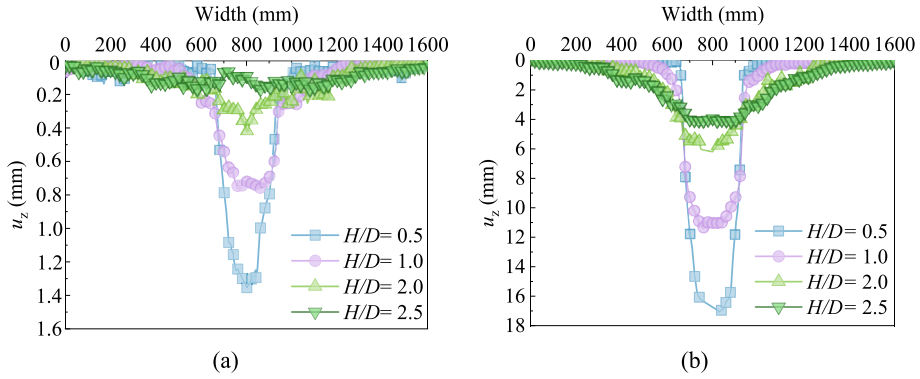

Fig. 15. Settlement troughs at the pile tip at different H/D. (a) $V_{l,t} = 0.84\%$, and (b) $V_{l,t} = 8.48\%$.

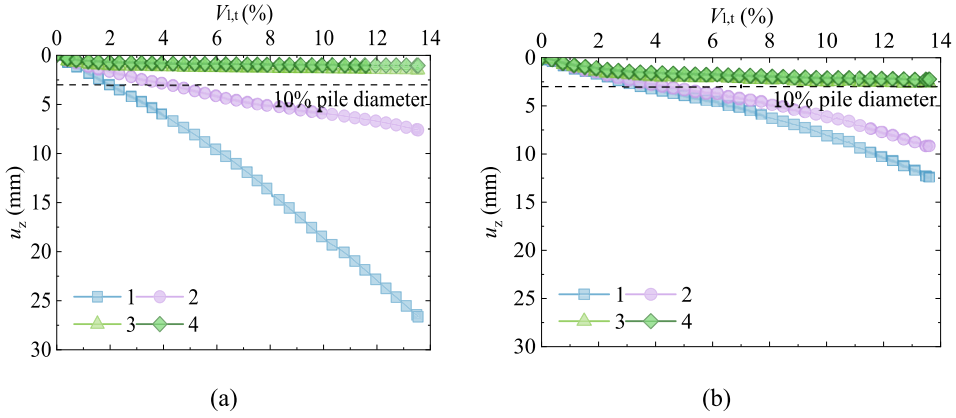

Fig. 16. Evolution of pile settlement with $V_{l,t}$ at different H/D values. (a) $H/D = 0.5$, and (b) $H/D = 2.0$.

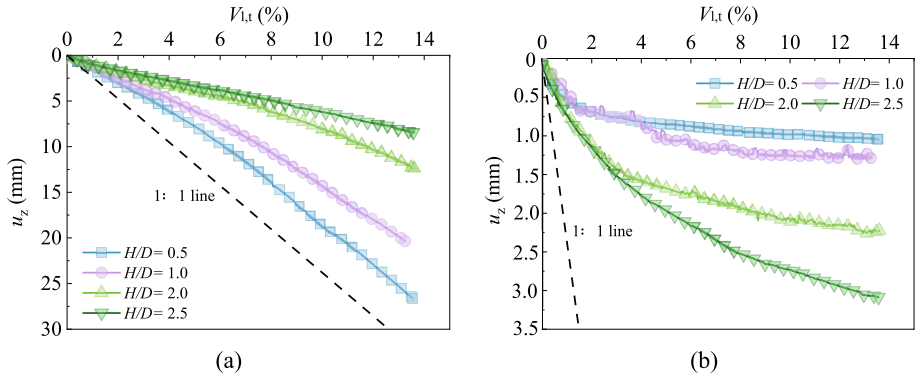

Fig. 17. Evolution of pile settlement with $V_{l,t}$. (a) Pile at tunnel centerline (Pile 1), and (b) pile at outside of the tunnel (Pile 4).

effective index called the settlement deflection ratio (DR) of the pile-raft foundation, which is defined as

$$\mathrm{DR} = (S_{\max} - S_{\min})/S_{\max}, \tag{1}$$

where $S_{\max}$ denotes the maximum pile settlement, and $S_{\min}$ represents the minimum pile settlement. When DR is zero, all piles settle equally, meaning there is no uneven settlement.

Figure 18(a) presents the DR with the ratio of H/D at different $V_{l,t}$. As the H/D increases, the tunneling-induced DR of the pile-raft foundation decreases. When $V_{l,t} = 0.84\%$, the reduction in settlement of the inner-side piles with increasing H/D results in a lower settlement difference between the inner and outer piles. Conversely, when $V_{l,t} = 8.48\%$, while the settlement of the inner-side piles decreases with H/D, the settlement of the outer-side piles increases. Otherwise, the DR increases with greater tunnel volume loss, as shown in Fig. 18(a), which is related to the variation of settlement rate with $V_{l,t}$ between the inner and outer piles.

The maximum settlement is normalized by the displacement of the trapdoor (δ), which represents the sensitivity of the soil displacement to the displacement of the tunnel-shaped trapdoor. Figure 18(b) presents the normalized maximum settlement evolution with H/D at different $V_{l,t}$.

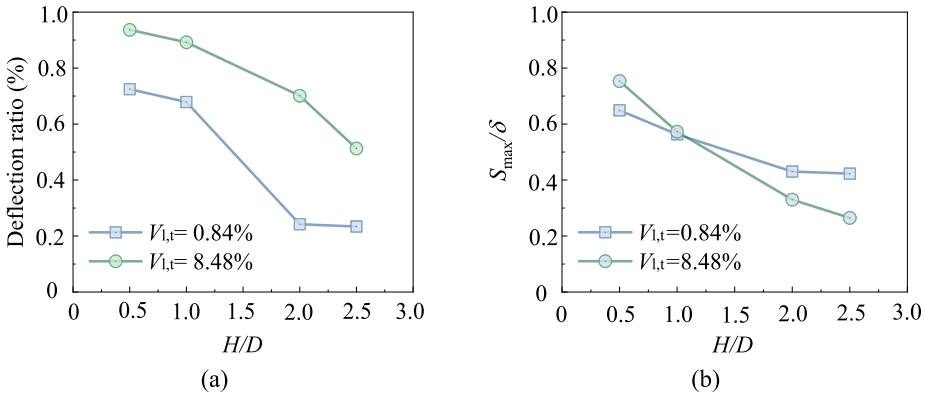

Fig. 18. Effect of H/D on the deformation of pile-raft structure under different tunnel volume loss. (a) DR of pile-raft foundation, and (b) normalized pile settlement.

The normalized pile settlement decreases significantly with the increasing H/D. There is a slight reduction in the normalized pile settlement rate with increasing H/D, which is associated with the formation of an arching structure in the ground.

3.3 Effects of ground surface load

Figures 19 and 20 present the tunneling-induced soil displacement fields and shear strain fields under different surface loads (P). As shown in Fig. 19(a) and 20(a), the tunneling-induced settlement pattern reaches the surface vertically ($\theta \approx 90°$), and the settlement width of the surface was $1D$ when $V_{l,t} = 0.84\%$. The tunneling-induced soil displacement pattern was similar under different P.

The tunneling-induced disturbed zone expands as the $V_{l,t}$ increases, and the settlement width of the surface was greater than the tunnel diameter, as shown in Fig. 19(b). The tunneling-disturbed zone expands with the increasing P, and the settlement width of the ground surface gradually increases from $2D$ to $4D$. When $P = 0$ kPa, the boundary of the tunneling-disturbed zone develops upward along the

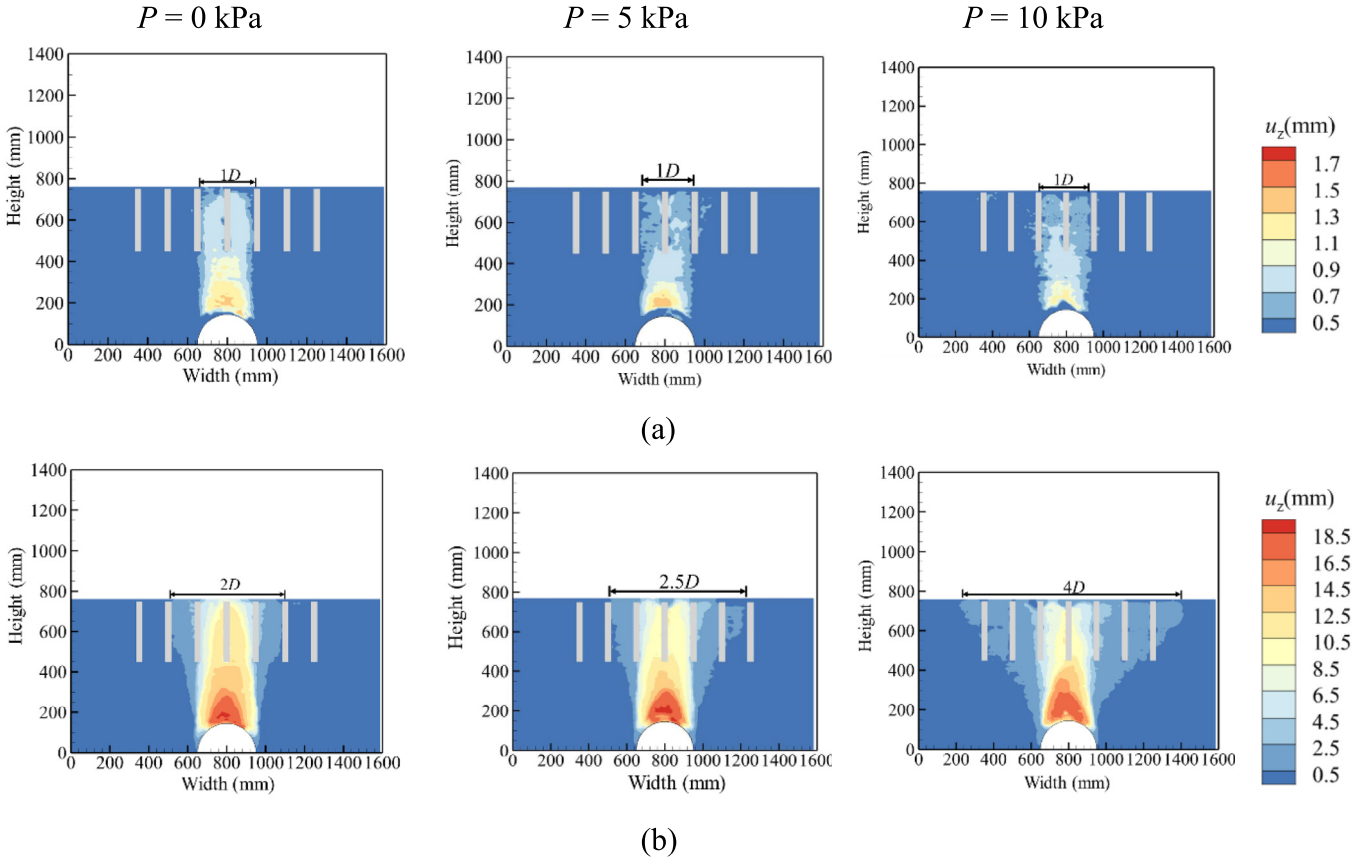

Fig. 19. Displacement fields with different values of P ($H/D = 1$). (a) $V_{l,t} = 0.84\%$, and (b) $V_{l,t} = 8.48\%$.

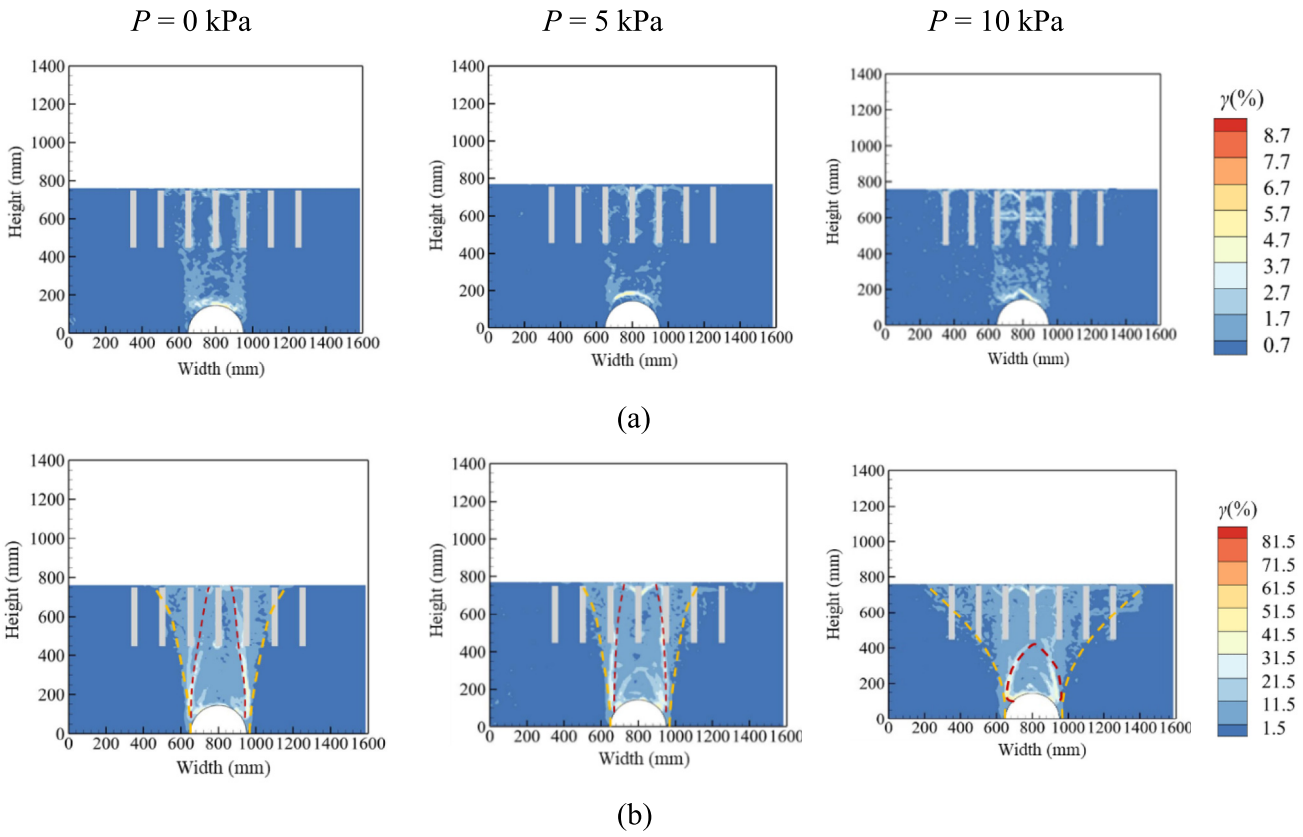

Fig. 20. Shear strain fields with different values of P ($H/D = 1$). (a) $V_{l,t} = 0.84\%$, and (b) $V_{l,t} = 8.48\%$.

pile to the surface, indicating that the pile reduces the lateral effect range and surface settlement width. However, the blocking effect of piles gradually diminishes with the increasing P. The settlement width of the ground surface was increased to $4D$ when $P = 10$ kPa. As shown in Fig. 20(b), the arch zone expands with the increasing P, which is associated with the larger compression zone on the surface of the foundation (Khatami et al., 2019). With the increasing P, the height of the loosened zone is reduced due to the greater confining stress (Iglesia et al., 2011).

Figure 21 presents the evolution of pile settlement with $V_{l,t}$ at different ground surface loads when $H/D = 1.0$. For inner-side Pile 1, the pile settlement rate was lower than the trapdoor displacement rate in the initial stage, and the settlement curve reached the 1:1 line in the ultimate stage, which indicates that P has a limited effect on the inner-side maximum pile settlement. However, for outer-side Pile 4, the pile settlement increases significantly with P. When $P = 0$ kPa, tunneling has limited effect on Pile 4 (see Fig. 21(b)). When $V_{l,t}$ is relatively large, the outer-side settlement gradually tends to stabilize.

Figure 22 presents the DR of a pile-raft foundation with P at different $V_{l,t}$. When $P = 0$ kPa, the DR is approximately 1 because the settlement of the outer-side piles is nearly zero (as shown in Fig. 21(b)). As P increases, the DR decreases significantly. This decrease occurs because higher P values increase the load distribution to the foundation outside the tunnel, leading to greater settlement of

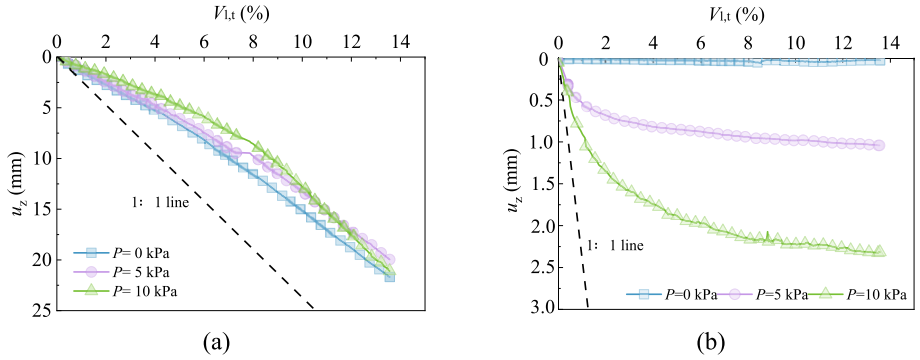

Fig. 21. Development of pile settlement with $V_{l,t}$ at different values of P ($H/D = 1.0$). (a) Pile 1, and (b) Pile 4.

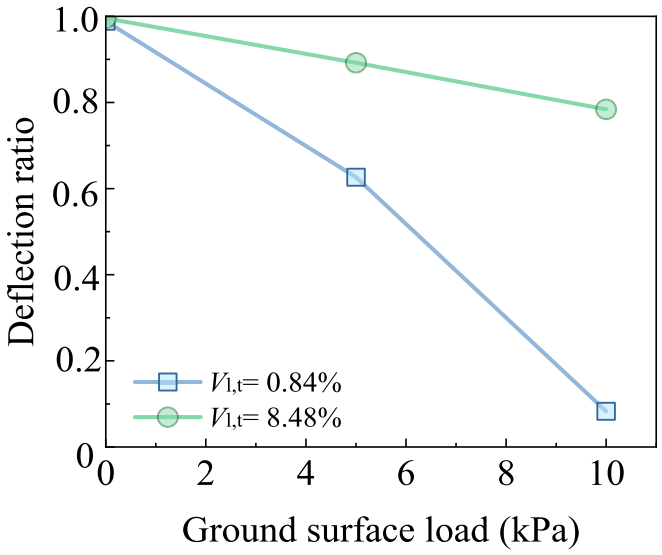

Fig. 22. DR changes with P for $V_{l,t}$ = 0.84% and 8.48%.

the outer-side piles. Further, Fig. 22 reveals that the DR of the pile-raft foundation increases with $V_{l,t}$ because the settlement rate of inner-side piles increases with $V_{l,t}$, whereas the settlement rate of outer-side piles decreases. In general, P has limited effect on the maximum pile settlement, but it can effectively reduce the DR of the pile-raft foundation.

4 Discussion

Pile settlement is the most important parameter for the serviceability analysis of piled structures (Chiang & Lee, 2007; Ng et al., 2013). The tunneling-induced pile settlement is affected by soil displacement which is closely related to the development of arching effects (Franza et al., 2019; Zhao et al., 2021; Wu et al., 2022). Soil arching effect helps explain (i) the transition from a narrow to a wide tunneling-induced soil displacement field with increasing tunnel burial depth and (ii) the expansion of the tunneling-induced soil displacement field with increasing $V_{l,t}$. Therefore, the arching effect should be given priority in the engineering of tunneling beneath the pile-raft foundation of HSR. The relationship between pile settlement behavior and progressive arching deformation was discussed in this section.

4.1 Relationship between pile settlement behavior and arching deformation

Significant differences exist in how tunneling-induced settlement characteristics affect piles in various types of tunneling-disturbed zones (Selemetas et al., 2005; He et al., 2022). Based on the presented experimental data, the maximum settlement occurs in the pile located on the tunnel centerline, which directly threatens the safety and stability of the pile-raft structure. According to the settlement behavior of the pile located on the tunnel centerline, three types of settlement patterns of tunneling-ground-pile systems can be identified, as shown in Fig. 23. It also illustrates the impact of arching effects on the tunneling-induced settlement pattern of pile-raft foundations.

The tunneling-induced settlement pattern of the pile-raft foundation depends on the relative position between the tunnel-pile distance and the height of the loosened zone. The pile settlement behavior in different areas of tunneling-disturbed zone can be divided into three types. (i) When the tunnel-pile distance is less than the height of the loosened zone, piles are in the loosened zone and the settlement pattern is shown in Fig. 23(a). (ii) When the tunnel-pile distance is greater than the height of the loosened zone, piles are in the arch zone and the settlement pattern is shown in Fig. 23(b). In these tests, the height of the loosened zone was determined by the distance between the intersection point of two clear bands and the tunnel crown. (iii) When the tunnel-pile distance was greater than the

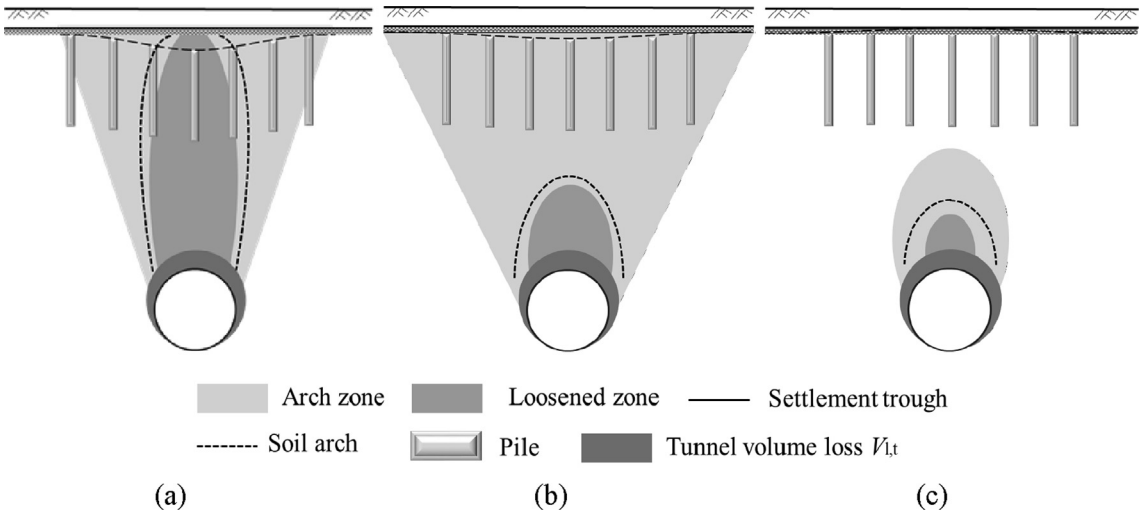

Fig. 23. Different tunneling-induced settlement patterns in pile-raft foundation. (a) Pile 1 in the loosened zone, (b) Pile 1 in the arch zone, and (c) Pile 1 in the undisturbed zone.

height of the arch zone, tunneling had a limited effect on the pile-raft foundation, and the settlement pattern was shown in Fig. 23(c). In the following section, combined with the soil stress and settlement behavior, the evolution of soil arching on the pile settlement behavior in the first two settlement patterns was discussed.

4.1.1 Piles in the loosened zone

When piles are in the loosened zone, as shown in Fig. 24 (a), arching affects a proportionally large zone of soil above the tunnel, resulting in a trumpet-like displacement field with narrow settlement troughs. Figure 24(b) shows the soil settlement trough and pile settlement at the pile tip elevation, where soil settlement exceeds pile settlement. This results in reduced bearing capacity of the pile foundation.

Figure 24(c) presents the u_z/δ versus h/D at different $V_{l,t}$. The normalized soil displacement is defined as the ratio of soil displacement (u_z) to the displacement of the trapdoor (δ). u_z/δ represents the sensitivity of the soil displacement propagation from the tunnel crown (or trapdoor position) to the pile tip. The horizontal axis represents the elevation (h) normalized by the tunnel diameter (D). Section S1 is the tunnel centerline, and Section S2 is 1.5D away from S1 (see Fig. 24(a)). As shown in Fig. 24(c), the displacement of soil above the tunnel centerline has almost the same displacement as the trapdoor, which indicates the soil is loosened, and thus can be judged that this area is the loosened zone. The u_z/δ in the loosened zone increases with the increasing $V_{l,t}$, which indicates that the surrounding soil is more susceptible to disturbances caused by tunnel construction due to the looser soil. Otherwise, the tunneling has limited effect on the soil outside the tunnel (S2).

Due to the shearing dilation or contraction of the sand with the development of $V_{l,t}$, the volume loss changes gradually along h (Lin et al., 2021). Therefore, a transmission ratio of ground volume loss (TRGVL) is defined as Eq. (2):

$$T(h) = \frac{V_s(h)}{\Delta V}. \tag{2}$$

TRGVL can represent the volume deformation features of the soil between the tunnel crown and h. For the dense sand, due to the dilatancy behavior of sand, there should be $0 < T(h) < 1$. This is consistent with the experimental results, as D_r is 70%. While, for loose sand, $T(h)$ will be larger than 1 for the contraction behavior of the loosened sand. Figure 24(d) shows that $T(h)$ decreases linearly with the increasing h, which indicates that the change of dilatancy volume is uniform along the elevation in the loosened zone. This change can be attributed to the expansion of the loosened zone to the surface, and the unformed arching structure is unable to prevent the propagation of the soil deformation.

The soil arching effect is a common stress transfer mechanism in sand, and the influence of the arching effect on the

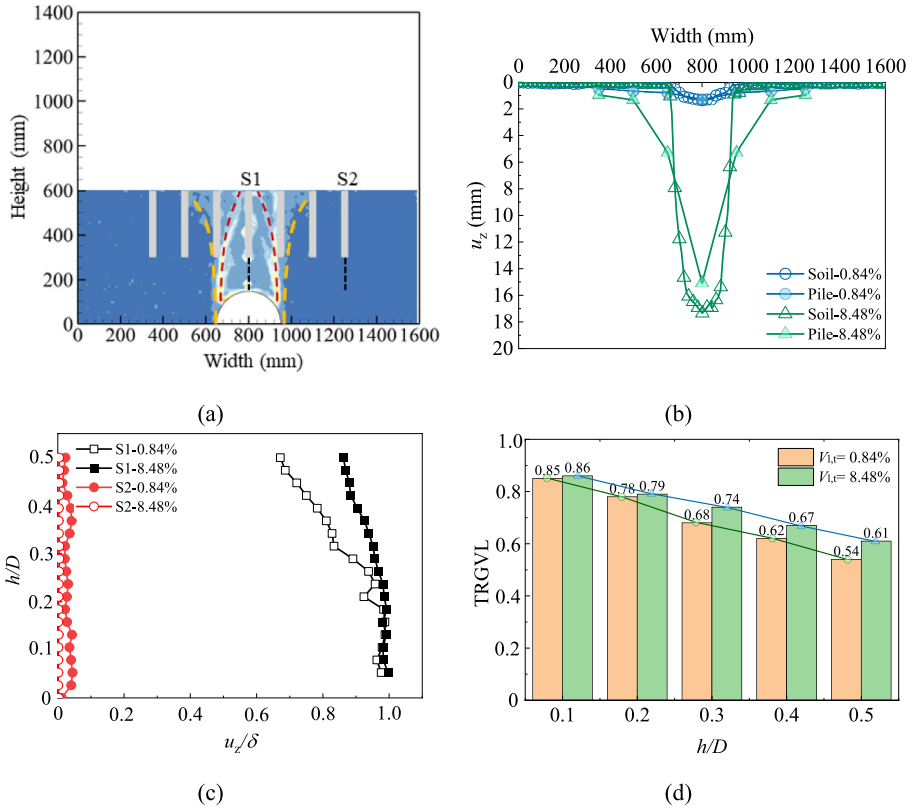

Fig. 24. Pile and soil displacement in the loosened zone ($H/D = 0.5$). (a) Shear strain field of Pile 1 in the loosened zone ($H/D = 0.5$), (b) soil settlement trough and pile settlement at pile tip elevation, (c) normalized soil displacement, and (d) TRGVL.

stress redistribution can be directly exacerbated by soil stress (Bi et al., 2019). Figure 25 presents the variation of vertical soil pressure (σ)-depth curves in the loosened zone at different $V_{l,t}$ when $H/D = 0.5$. The soil stress at the pile tip was very small in S1, which indicates that voiding occurs above the soil at the bottom of the pile. The vertical stress in the soil above the tunnel center gradually transfers towards the soil outside the tunnel with increasing $V_{l,t}$.

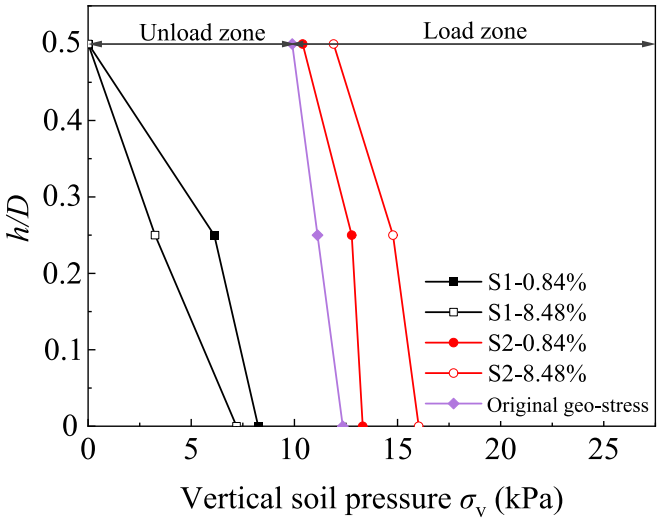

Fig. 25. Variation of σ-depth curves in loosened zone.

4.1.2 Piles in the arch zone

If piles are in the arch zone, a soil arching structure is formed beneath the pile tip, as shown in Fig. 26(a). The tunneling-disturbed zone extends to the ground surface, resulting in wider settlement troughs at the surface. As shown in Fig. 26(b), the pile settlement is consistent with the soil settlement at the pile tip elevation, and tunneling-induced uneven settlement of piles in pile-raft foundation. This pattern is significantly different from the situation where the pile is in the loosened zone (see Fig. 24(b)).

Figure 26(c) presents the u_z/δ with the increasing h. Two sections, S1 and S2, and two $V_{l,t}$, 0.84%, and 8.48% were selected to better demonstrate the role of the arch effect. (i) At Section S1, for $V_{l,t} = 0.84\%$, the soil displacement increases linearly with the increasing h when $0.5 < H/D < 2.0$ (Zone I). The soil displacement increases significantly when $0 < H/D < 0.5$, which is due to the unformed arching structure. Therefore, the height of the loosened zone was $0.5D$. As $V_{l,t}$ increases from 0.84% to 8.48%, the height of the loosening zone increases from $0.5D$ to $1.0D$. (ii) At Section S2, the settlement range is closed at the pile tip, which is consistent with the results shown in Fig. 26(a). The u_z/δ at S2 decreases with the increasing $V_{l,t}$.

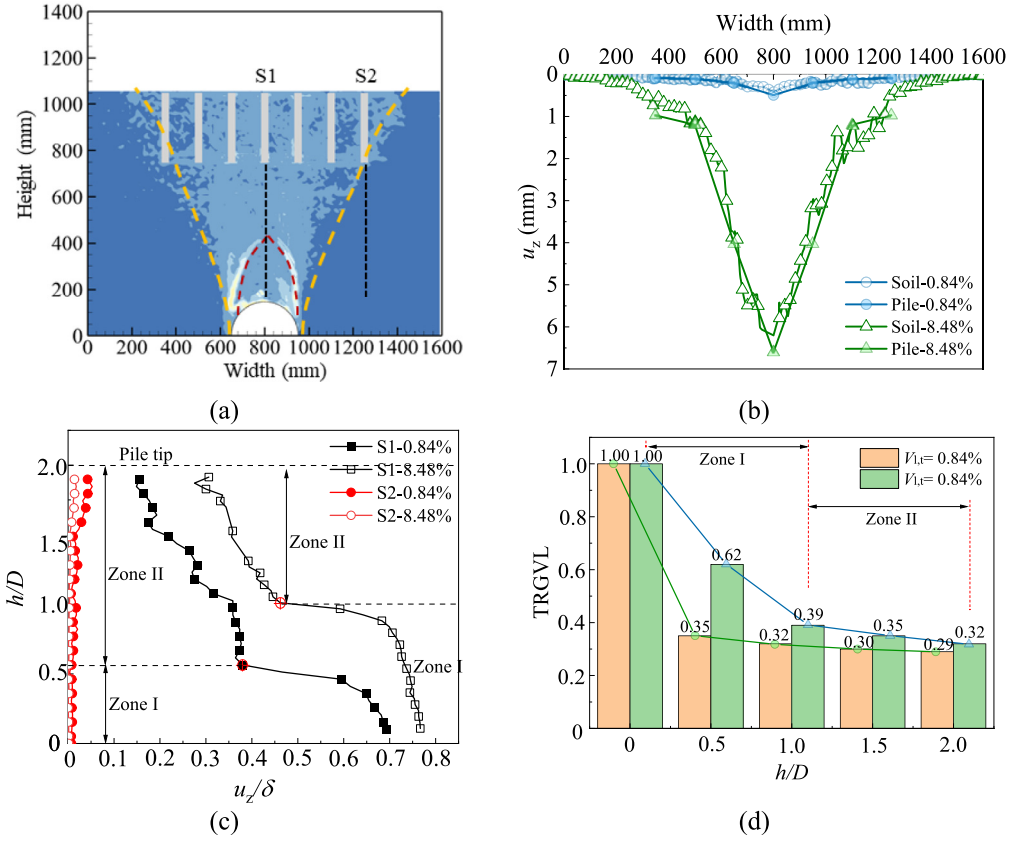

Fig. 26. Pile and soil displacement in the arch zone ($H/D = 2.0$). (a) Shear strain field of Pile 1 in the arch zone ($H/D = 2.0$), (b) soil settlement trough and pile settlement at pile tip elevation, (c) normalized soil displacement, and (d) TRGVL.

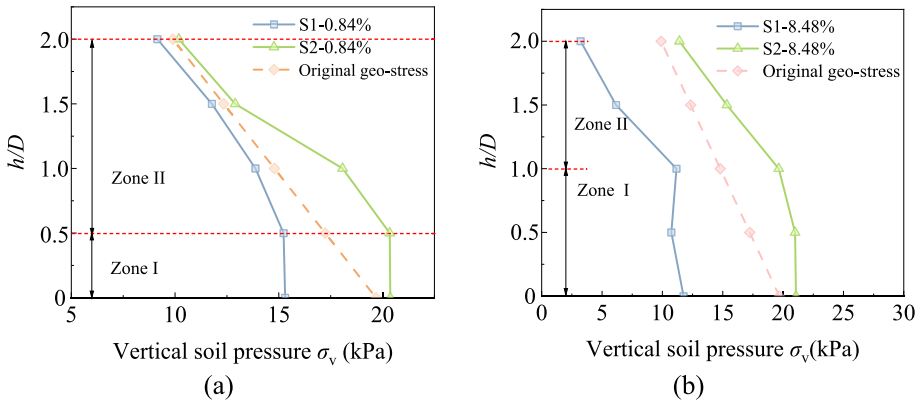

Fig. 27. Variation of σ-depth curves during tunneling. (a) $V_{l,t} = 0.84\%$, and (b) $V_{l,t} = 8.48\%$ ($H = 2.0D$, $P = 5$ kPa).

Figure 26(d) presents TRGVL along h/D. One can see that $T(h)$ decreases nonlinearly with the increasing h. TRGVL decreases linearly with the increasing H/D in the loosened zone (Zone I), whereas the TRGVL decreases slightly with the increasing H/D in the arch zone (Zone II). This phenomenon indicates that an arching structure formed at the upper part of the loosened zone can effectively reduce the propagation of soil deformation.

Figuer 27(a) presents the variation of σ-depth curves at different $V_{l,t}$ when $H/D = 2.0$. Based on the σ-depth curves, we classify two tunneling-disturbed zones. (i) $0.5 < H/D < 2.0$ in Fig. 27(a) and $1.0 < H/D < 2.0$ in Fig. 27(b): The increase in σ_v with depth becomes nonlinear. Compared with the initial earth pressure, the soil stress decreases in S1, whereas the soil stress increases in S2. This indicates that the soil stress above the tunnel is transferred to the soil on both sides of the tunnel (Chen et al., 2011). Therefore, the monitoring section (Zone II) was located in the arch zone at this time. (ii) $0 < h/D < 0.5$ in Fig. 27(a) and $0 < h/D < 1.0$ in Fig. 27(b): σ_v decreases or remains with the increasing h/D, indicating that the soil mass in this zone may be in a loosened state (Lin et al., 2019). Otherwise, the height of the loosened zone increases with an increasing $V_{l,t}$.

In summary, arching effect has a significant impact on the soil displacement of pile-raft foundations and the deflection of pile-raft structures during tunnel construction. By leveraging the soil arching effect and optimizing factors such as tunnel-pile distance, ground loads, and tunnel volume loss, the stability and performance of pile-raft foundations near tunneling activities can be effectively ensured.

4.2 Limitations and future works

In this study, the tunneling-induced deformation characteristics of pile-raft foundations were observed using PIV and LVDTs. However, there are still some limitations to this study. (i) Mobilisation mechanism: The discrete element method will be used to elaborate on the impact of the soil arching effect on the tunneling-induced deformation mechanisms of pile-raft foundations from a microscopic perspective in future work. (ii) Structural parameters of pile-supported foundations: Factors such as different pile spacing and pile installation methods can all affect the tunneling-induced settlement characteristics of pile foundations. (iii) Dynamic load: The effects of dynamic loads on soil arching and soil settlement are also worth considering. The evolution process of the soil arching effect and soil settlement is affected by dynamic loading (Bi et al., 2019; Dai et al., 2022; Ye et al., 2022; He et al., 2024), which is of great significance for tunneling beneath operating railway lines. (iv) From 1g test to engineering application: Charts summarizing pile settlements, deflection ratio, and critical tunnel volume losses were presented based on our experimental data. The data were also described to assess the tunneling-induced damage of pile-raft foundations. Appropriate judgments should be made before applying these outcomes to real cases, which may differ considerably from the conditions considered in the tests presented here.

4.3 Discussion on practical implications

Despite the limitations described above, our study on the tunneling-induced deformation characteristics of the pile-raft foundation offers valuable insights into how tunneling affects these structures. The findings can contribute to the following areas of risk assessment and mitigation strategies. (i) Optimized design and construction strategies: Based on the understanding of the pile-soil deformation characteristics caused by tunneling, engineers can design more optimized construction plans and strategies. These may include appropriately increasing the synchronous grouting pressure and grouting volume to minimize the impact of tunnel construction on HSR infrastructure by controlling ground loss. For example, during the stage of low tunnel volume loss, the soil and pile above the tunnel center should be the key monitoring areas. As tunnel construction progresses and the disturbed zone gradually expands, the settlement of the pile and soil outside the tunnel center should be also monitored. (ii) Development of

emergency response plans: Understanding deformation characteristics can also contribute to the development of emergency response plans. For example, when the tunnel volume loss is low, excessive settlement deformation of the subgrade is mainly concentrated in the area above the tunnel center, and targeted settlement lifting measures can be taken accordingly. As tunnel construction progresses and the disturbed zone expands, settlement monitoring should be conducted and maintenance preparations should be made for the entire tunnel construction area.

5 Conclusions

A model testing device was developed to study the tunneling-induced deformation behavior of pile-raft foundations. The effects of the distance between the tunnel and pile tip and surface load were also considered. The key findings of this study can be summarized as follows.

(1) The tunneling-disturbed zone was divided into the loosened zone, arch zone, and undisturbed zone based on the observed shear band and soil displacement, and significant settlement occurs in the loosened zone. Compared with the tunneling-disturbed zone in the greenfield, the pile-raft foundation reduces the range of the arch zone due to the blocking effect of the piles, while increasing the range of the loosened zone.
(2) The distance between the tunnel and pile tip (H/D) had a significant effect on the displacement of soil and piles. The arch zone expands with the increasing H/D, which results in the larger settlement of the outer-side piles, and the height of the loosened zone gradually decreases to approximately $1.0D$. When $H/D > 2.0$, the height of the loosened zone shows little variation. When the piles are in the loosened zone, the pile settlement with tunnel volume loss is similar to the trapdoor displacement rate. The pile settlement decreases significantly with the increasing tunnel-pile distance when piles are in the loosened zone, whereas the pile settlement decreases slightly when piles are in the arch zone.
(3) The ground surface load (P) had limited effect on the settlement of the pile at the tunnel centerline. As P increases, the settlement of the outer-side pile increases significantly due to the larger tunneling-disturbed zone and the deflection ratio (DR) of the pile-raft foundation decreases.
(4) The progressive arching deformation has significantly affected the tunneling-induced soil deformation and pile settlement behavior in the pile-raft foundation. According to the relative position between the piles and the formed arch structure, three patterns of tunneling-ground-pile systems can be identified. (i) Piles in the loosened zone: The soil settlement exceeds pile settlement at the pile tip elevation, which causes the loss of the pile tip resistance and reduces the bearing capacity of the pile-raft foundation. (ii) Piles in the arch zone: The tunneling-induced pile settlement is similar to the soil deformation at the pile tip, and the formed arching structure above the tunnel can effectively reduce the propagation of the soil volume loss. (iii) Piles in the undisturbed zone: Tunneling has a limited effect on the pile-raft foundation.

Data availability

The data that support the findings of this study are available from the corresponding author upon reasonable request.

CRediT authorship contribution statement

Botao Hu: Writing – review & editing, Writing – original draft, Visualization, Software, Methodology, Investigation, Conceptualization. **Yao Shan:** Supervision, Funding acquisition, Conceptualization. **Yu Zhao:** Writing – review & editing, Software, Funding acquisition. **Binglong Wang:** Writing – review & editing, Funding acquisition. **Shunhua Zhou:** Supervision. **Giovanni S. Alberti:** Validation. **Wenjie Ma:** Visualization. **Bettina Detmann:** Investigation. **Laurent Briançon:** Resources.

Declaration of competing interest

The authors declare that they have no known competing financial interests or personal relationships that could have appeared to influence the work reported in this paper.

Acknowledgement

This research was supported by the National Natural Science Foundation of China (Grant No. 52378458), the National Postdoctoral Program for Innovative Talent of China (Grant No. BX20230233), the Fundamental Research Funds for the Central Universities (Grant No. 22120230311), Special Funds of the Tongji University for "Sino-German Cooperation 2.0 Strategy", Guangdong Basic and Applied Basic Research Foundation of China (Grant No. 2023A1515110047), the MIUR Excellence Department Project awarded to Dipartimento di Matematica, Università di Genova, CUP D33C23001110001, and the European Union - Next Generation EU.

References

Amorosi, A., Boldini, D., De Felice, G., Malena, M., & Sebastianelli, M. (2014). Tunnelling-induced deformation and damage on historical masonry structures. *Géotechnique, 64*(2), 118–130.

Bhartiya, P., Chakraborty, T., & Basu, D. (2021). Prediction of piled raft settlement using soil subgrade modulus in consolidating clays. *Practice Periodical on Structural Design and Construction, 26*(4), 04021037.

Bi, Z. Q., Gong, Q. M., Guo, P. J., & Cheng, Q. (2019). Experimental study of the evolution of soil arching effect under cyclic loading based on trapdoor test and particle image velocimetry. *Canadian Geotechnical Journal, 57*(6), 903–920.

Bolton, M. D., Gui, M. W., Garnier, J., Corte, J. F., Bagge, G., Laue, J., & Renzi, R. (1999). Centrifuge cone penetration tests in sand. *Géotechnique, 49*(4), 543–552.

Boonsiri, I., & Takemura, J. (2015). Observation of ground movement with existing pile groups due to tunneling in sand using centrifuge modelling. *Geotechnical and Geological Engineering, 33*, 621–640.

Cao, L. Q., Chen, X. S., Lu, D. C., Zhang, D. L., & Su, D. (2024). Theoretical prediction of ground settlements due to shield tunneling in multi-layered soils considering process parameters. *Underground Space, 16*(1), 29–43.

Chen, C. N., Huang, W. Y., & Tseng, C. T. (2011). Stress redistribution and ground arch development during tunneling. *Tunnelling and Underground Space Technology, 26*(1), 228–235.

Chiang, K., & Lee, C. (2007). Responses of single piles to tunneling-induced soil movements in sandy ground. *Canadian Geotechnical Journal, 44*(10), 1224–1241.

Cheng, C. Y. (2003). Finite element study of tunnel-soil-pile interaction. [Master's thesis, National University of Singapore, Singapore].

Dai, N., Shan, Y., Fu, L. L., Ye, W. T., Guo, P. J., Zhou, S. H., Rackwitz, F., & Stolle, D. (2022). Vibro-fluidization of sand under coupled static loading and high-frequency cyclic loading. *Canadian Geotechnical Journal, 59*(1), 101–110.

da Silva Burke, T. S., & Elshafie, M. Z. (2021). Arching in granular soils: experimental observations of deformation mechanisms. *Géotechnique, 71*(10), 866–878.

Franza, A., Marshall, A. M., & Zhou, B. (2019). Greenfield tunnelling in sands: the effects of soil density and relative depth. *Géotechnique, 69*(4), 297–307.

Franza, A., & Marshall, A. M. (2018). Centrifuge modeling study of the response of piled structures to tunneling. *Journal of Geotechnical and Geoenvironmental Engineering, 144*(2), 04017109.

Franza, A., & Marshall, A. M. (2019). Centrifuge and real-time hybrid testing of tunneling beneath piles and piled buildings. *Journal of Geotechnical and Geoenvironmental Engineering, 145*(3), 04018110.

Gardina, G., Dejong, M. J., & Mair, R. J. (2015). Interaction between surface structures and tunnelling in sand: Centrifuge and computational modelling. *Tunneling and Underground Space Technology, 50*, 465–478.

Han, X. F. (2020). Influence of shield tunneling on the ballastless subgrade of shanghai-nanjing intercity railway. *Railway Construction Technology, 5*, 137–142 (in Chinese).

He, S. Y., Lai, J. X., Li, Y., Wang, K., Wang, L. X., & Zhang, W. M. (2022). Pile group response induced by adjacent shield tunnelling in clay: Scale model test and numerical simulation. *Tunnelling and Underground Space Technology, 120*, 104039.

He, C., Jia, Y. P., & Zhou, S. H. (2024). Semi-analytical method for calculating ground vibrations from a tunnel in a homogeneous half-space with an irregular surface. *Journal of Sound and Vibration, 591*, 118615.

Huo, J. S., Wang, B. L., & Zhou, S. H. (2011). Safety Analysis of foundation reinforcement scheme for shield tunnel under-passing intercity railway. *China Railway Science, 32*(5), 71–77 (in Chinese).

Hong, Y., Soomro, M. A., Ng, C. W. W., Wang, L. Z., Yan, J. J., & Li, B. (2015). Tunnelling under pile groups and rafts: Numerical parametric study on tension effects. *Computers and Geotechnics, 68*, 54–65.

Hu, B. T., Shan, Y., Zhao, Y., Wang, B. L., Zhou, S. H., Alberti, G. S., Ma, W. J., & Detmann, B. (2024). Experimental study on tunneling-induced soil arching evolution in pile-raft foundations. *Transportation Geotechnics, 48*, 101340.

Iglesia, G. R., Einstein, H. H., & Whitman, R. V. (2011). Validation of centrifuge model scaling for soil systems via trapdoor tests. *Journal of Geotechnical and Geoenvironmental Engineering, 137*(11), 1075–1089.

Jongpradist, P., Kaewsri, T., Sawatparnich, A., Suwansawat, S., Youwai, S., Kongkitkul, W., & Sunitsakul, J. (2013). Development of tunneling influence zones for adjacent pile foundations by numerical analyses. *Tunnelling and Underground Space Technology, 34*, 96–109.

Kaalberg, F. J., Teunissen, E. A. H., Van Tol, A. F., & Bosch, J. W. (2006). Dutch research on the impact of shield tunnelling on pile foundations. *In Proceedings of the 16th International Conference on Soil Mechanics and Geotechnical Engineering (pp. 1615–1620)*. Osaka, Japan.

Khatami, H., Deng, A., & Jaksa, M. (2019). An experimental study of the active arching effect in soil using the digital image correlation technique. *Computers and Geotechnics, 108*, 183–196.

Khatami, H., Deng, A., & Jaksa, M. (2020). Passive arching in rubberized sand backfills. *Canadian Geotechnical Journal, 57*(4), 549–567.

Khatami, H., Deng, A., & Jaksa, M. (2021). Mapping soil arching-induced shear and volumetric strains in dense sands. *Transportation Geotechnics, 28*, 100547.

Lai, H. J., Zheng, J. J., Zhang, R. J., & Cui, M. J. (2018). Classification and characteristics of soil arching structures in pile-supported embankments. *Computers and Geotechnics, 98*, 153–171.

Lin, Q. T., Tian, Y., Lu, D. C., Gong, Q. M., Du, X. L., & Gao, Z. W. (2021). A prediction method of ground volume loss variation with depth induced by tunnel excavation. *Acta Geotechnica, 16*, 3689–3707.

Lin, X. T., Chen, R. P., Wu, H. N., & Cheng, H. Z. (2019). Three-dimensional stress-transfer mechanism and soil arching evolution induced by shield tunneling in sandy ground. *Tunnelling and Underground Space Technology, 93*, 103104.

Lim, C. X., Jusoh, S. N., Lim, C. B., Abdullah, R. A., & Yunus, N. Z. M. (2023). Tunnel depth effect to pile in Tunnel's influence zone. *Physics and Chemistry of the Earth, Parts A/B/C, 129*, 103298.

Liu, C. Y., Shan, Y., Wang, B. L., Zhou, S. H., & Wang, C. D. (2022). Reinforcement load in geosynthetic-reinforced pile-supported model subgrades. *Geotextiles and geomembranes, 50*(6), 1135–1146.

Lu, H., Shi, J. W., Ng, C. W. W., & Lyu, Y. R. (2020). Three-dimensional centrifuge modeling of the influence of side-by-side twin tunneling on a piled raft. *Tunnelling and Underground Space Technology, 103*, 103486.

Marshall, A. M., Farrell, R. P., Klar, A., & Mair, R. (2012). Tunnels in sands: The effect of size, depth and volume loss on greenfield displacements. *Géotechnique, 62*(5), 385–399.

Ng, C. W. W., Lu, H., & Peng, S. Y. (2013). Three-dimensional centrifuge modelling of the effects of twin tunnelling on an existing pile. *Tunneling and Underground Space Technology, 35*, 189–199.

Ng, C. W. W., Soomro, M. A., & Hong, Y. (2014). Three-dimensional centrifuge modelling of pile group responses to side-by-side twin tunnelling. *Tunnelling and Underground Space Technology, 43*, 350–361.

National Railway Administration of the People's Republic of China (2017). *TB 10182—2017: Technical Specification for Highway and Municipal Engineering under Crossing High Speed Railway*. Beijing, China: China Railway Publishing House (in Chinese).

Ong, C. W., Leung, C. F., Yong, K. Y., & Chow, Y. K. (2007). Performance of pile due to tunneling-induced soil movements. *In Underground space—the 4th dimension of metropolises (pp. 619–624)*. CRC Press.

Rui, R., Van Tol, A. F., Xia, Y. Y., Van Eekelen, S. J. M., & Hu, G. (2016). Investigation of soil-arching development in dense sand by 2D model tests. *Geotechnical Testing Journal, 39*(3), 415–430.

Selemetas, D., Stangding, J. R., & Mair, R. J. (2005). The Response of Full-scale Piles and Piled Structures to Tunnelling. In *Proceedings of the 5th International Conference of TC 28 of the ISSMGE* (pp. 763–769).

Shan, Y., Cheng, G. H., Gu, X. Q., Zhou, S. H., & Xiao, F. Z. (2021). Optimization of design parameters of displacement isolation piles constructed between a high-speed railway bridge and a double-line metro tunnel: From the view point of vibration isolation effect. *Computers and Geotechnics, 140*, 104460.

Shan, Y., Xiao, W. X., Xiang, K., Wang, B. L., & Zhou, S. H. (2022). Semi-automatic construction of pile-supported subgrade adjacent to existing railway. *Automation in Construction, 134*, 104085.

Shan, Y., Li, X. R., & Zhou, S. H. (2023). Multi-objective optimisation methodology for stiffness combination design of bridge-embankment transition zones in high-speed railways. *Computers and Geotechnics, 155*, 105242.

Wang, G. K., Shan, Y., Detmann, B., & Lin, W. F. (2024). Physics-Informed Neural Network (PINN) model for predicting subgrade settlement induced by shield tunnelling beneath an existing railway subgrade. *Transportation Geotechnics, 49*, 101409.

Wei, G. (2010). Selection and distribution of ground loss ratio induced by shield tunnel construction. *Chinese Journal of Geotechnical Engineering, 32*(9), 1354–1361 (in Chinese).

Wu, Y. J., Zhao, Y., Gong, Q. M., Zornberg, J. G., Zhou, S. H., & Wang, B. L. (2022). Alternant active and passive trapdoor problem: from experimental investigation to mathematical modeling. *Acta Geotechnica, 17*(7), 2971–2994.

Ye, W. T., Fu, L. L., Shan, Y., Dai, N., Guo, P. J., Zhou, S. H., & Rackwitz, F. (2022). Experimental study on dynamic characteristics of granular materials under axial high-frequency vibration. *Acta Geotechnica, 17*(6), 3211–3227.

Yuan, B. X., Chen, W. W., Jiang, T., Wang, Y. X., & Chen, K. P. (2013). Stereo particle image velocimetry measurement of 3D soil deformation around laterally loaded pile in sand. *Journal of Central South University, 20*(3), 791–798.

Yuan, B. X., Xu, K., Wang, Y. X., Chen, R., & Luo, Q. Z. (2017). Investigation of Deflection of a Laterally Loaded Pile and Soil Deformation Using the PIV Technique. *International Journal of Geomechanics, 17*(6), 04016138.

Zhao, Y., Gong, Q. M., Wu, Y. J., Tian, Z. Y., Zhou, S. H., & Fu, L. L. (2021). Progressive failure mechanism in granular materials subjected to an alternant active and passive trapdoor. *Transportation Geotechnics, 28*, 100529.

Zhou, B. (2015). Tunnelling-induced ground displacements in sand. [Doctoral dissertation, University of Nottingham, UK].

Zhou, S. H., Shan, Y., Wu, Z. Y., Zhao, W., Yang, L. C., & Lin, Y. W. (2023). Lateral deformation of high-speed railway foundation induced by adjacent subgrade construction in soft soils: Numerical and field study. *Transportation Geotechnics, 41*, 101005.